Neuroscience 116 (2003) 599–616

INCREASED DENDRITIC EXCITABILITY IN HIPPOCAMPAL CA1 *IN VIVO* IN THE KAINIC ACID MODEL OF TEMPORAL LOBE EPILEPSY: A STUDY USING CURRENT SOURCE DENSITY ANALYSIS

K. WU AND L. S. LEUNG*

Departments of Clinical Neurological Sciences and Physiology, University of Western Ontario, London, ON, Canada N6A 5A5

Abstract—We used kainic acid in rats as an animal model of temporal lobe epilepsy, and studied the synaptic transmission in hippocampal subfield CA1 of urethane-anesthetized rats *in vivo*. Dendritic currents were revealed by field potential mapping, using a single micropipette or a 16-channel silicon probe, followed by current source density analysis. We found that the population excitatory postsynaptic potentials in the basal dendrites and distal apical dendrites of CA1 were increased in kainate-treated as compared with control rats following paired-pulse, but not single-pulse, stimulation of CA3b or medial perforant path. In contrast, the trisynaptic midapical dendritic response in CA1 following medial perforant path stimulation was decreased in kainate-treated as compared with control rats. Increased coupling between excitatory postsynaptic potential and the population spike in CA1 was found after kainate seizures. Short-latency, presumably monosynaptic CA1 population spikes following medial perforant path stimulation was found in kainate-treated but not control rats. An enhancement of dendritic excitability was evidenced by population spikes that invaded into or originated from the distal apical dendrites of CA1 in kainate-treated but not control rats. Reverberation of hippocampo-entorhinal activity was evidenced by recurrent excitation of CA1 following CA3b stimulation in kainate-treated but not control rats. Blockade of inhibition by intraventricularly administered bicuculline induced excitatory potentials in CA1 that were stronger and more prolonged in kainate-treated than control rats. The bicuculline-induced excitation was mainly blocked by non-*N*-methyl-D-aspartate receptor antagonists.

We conclude that kainate seizures induced disinhibition in CA1 that unveiled excitation at the basal and distal apical dendrites, resulting in enhancement of the direct entorhinal cortex to CA1 input and reverberations via the hippocampo-entorhinal loop. These changes in the output of the hippocampus from CA1 are likely detrimental to the behavioral functions of the hippocampus and they may contribute to increased seizure susceptibility after kainate seizures.

Key words: seizures, CA3, entorhinal cortex, inhibition, dendritic spike, reverberation.

In temporal lobe epilepsy (TLE), seizures often arise from the hippocampus in the mesial temporal lobe. The causes of the seizure susceptibility are not clearly understood. Since a seizure involves populations of neurons, we believe that one contributing factor to seizure susceptibility is the increase in excitability of the neural circuit that involves the entorhinal cortex (EC) and the hippocampus.

The EC provides processed sensory inputs to the hippocampus through the perforant path, which projects to the dentate gyrus (DG) as well as to CA3 and CA1 (Witter et al., 2000). The DG in turn projects to CA3 through mossy fibers, and CA3 to CA1 through association and commissural fibers. CA1 projects back to the EC, directly or indirectly through the subiculum, and this completes a series of nested EC–hippocampus circuit loops.

At the first synapse of the longest EC–hippocampal circuit, the DG, neuronal inhibition appears to be increased in TLE patients (Wilson et al., 1998) and in different models of TLE, including kindling (Nusser et al., 1998; Otis et al., 1994; Tuff et al., 1983), kainic acid (KA) and pilocarpine models (Brooks-Kayal et al., 1998; Gibbs et al., 1997; Milgram et al., 1991). We and others have suggested that the enhanced inhibition in the DG may normally suppress seizures (Lothman, 1994; Wu and Leung, 2001), although we have proposed that this increased inhibition was fragile (Wu and Leung, 2001). Alternatively, others have proposed that mossy fiber sprouting (MFS) in the DG of human TLE or animal models contributes to the increased neuronal excitability and seizures (Golarai and Sutula, 1996; Okazaki et al., 1999; Wuarin and Dudek, 2001). We did not find MFS to correlate positively with excitability in the DG following KA treatment (Wu and Leung, 2001), and increased seizure susceptibility has been reported without MFS (Longo and Mello, 1998).

Relatively little is known about the strength of the DG to CA3 connection following TLE models, although sprouting of mossy fibers may occur in stratum oriens of CA3 (Ad-

*Corresponding author. Tel: +1-519-663-3733; fax: +1-519-663-3753.
E-mail address: sleung@uwo.ca (L. Leung).

Abbreviations: CSF, artificial cerebrospinal fluid, AEPs, average evoked potentials; ANCOVA, analysis of covariance, ANOVA, analysis of variance; CNQX, 6-cyano-7-nitroquinoxaline-2,3-dione, CSD, current source density; D-AP5, D-2-amino-5-phosphonopentanoic acid, DG, dentate gyrus; EC, entorhinal cortex, EPSP, excitatory postsynaptic potential; EPSP1, the slope of the population excitatory postsynaptic potential after the first pulse of a pair of pulses, EPSP2, the slope of the population excitatory postsynaptic potential after the second pulse of a pair of pulses; E-S, excitatory postsynaptic potential to spike, i.c.v., intracerebroventricular; IPI, interpulse interval, I/O, input/output; KA, kainic acid, LTP, long-term potentiation; MFS, mossy fiber sprouting, MPP, medial perforant path; NMDA, *N*-methyl-D-aspartate, PPF, paired-pulse facilitation; PPR, paired-pulse response ratio, PS, population spike; PS1, population spike after the first pulse of a pair of pulses, PS2, population spike after the second pulse of a pair of pulses; SLM, stratum lacunosum-moleculare, SO, stratum oriens; SP, stratum pyramidale, SR, stratum radiatum; str., stratum, TLE, temporal lobe epilepsy.

0306-4522/03$30.00+0.00 © 2003 Published by Elsevier Science Ltd on behalf of IBRO.
doi:10.1016/S0306-4522(02)00567-5

ams et al., 1997). Recurrent excitation in CA3 was decreased after KA treatment (Wu and Leung, 2001), presumably because of a loss in CA3 neurons. However, CA3 recurrent excitation was enhanced in a model of posttraumatic epilepsy (McKinney et al., 1997).

Many studies have addressed the changes in hippocampal CA1 following TLE models. CA1 neuronal excitability was increased after KA treatment in rats (Ashwood et al., 1986; Ashwood and Wheal, 1986; Franck and Schwartzkroin, 1985), partly because of increased excitatory postsynaptic potentials (EPSPs) (Ashwood and Wheal, 1986; Simpson et al., 1991; Turner and Wheal, 1991) and sprouting of recurrent axon collaterals of CA1 pyramidal cells (Esclapez et al., 1999; Nadler et al., 1980; Perez et al., 1996). In addition, a decrease in inhibition in CA1 contributed to an increase in paired-pulse excitability *in vivo* (Ashwood and Wheal, 1986; Cornish and Wheal, 1989; Franck et al., 1988; Franck and Schwartzkroin, 1985). The decrease in inhibition may be caused by a selective loss of GABAergic, parvalbumin- and somatostatin-containing interneurons (Best et al., 1993; Best et al., 1994), and a decreased expression of $GABA_A$ receptors (Tsunashima et al., 1997). However, there are also reports that some types of $GABA_A$ receptor-mediated inhibition were functionally intact in CA1 of KA-treated rats (Cossart et al., 2001; Williams et al., 1993), except for the feedforward inhibition in the stratum lacunosum-moleculare (SLM) of CA1 (Morin et al., 1998).

We are interested in the alterations of functional connections of the EC–hippocampal circuit following a model of TLE (Canning et al., 2000; Leung et al., 1998). These functional connections are not provided by studies on the hippocampal slice *in vitro*, which constitute the majority of the studies reviewed above. The hippocampal slice *in vitro* is disconnected from subcortical and (most) cortical inputs, and it has relatively smaller inhibition as compared with a preparation *in vivo* (Buckmaster and Schwartzkroin, 1995).

We studied the functional electrophysiology of CA1 in urethane-anesthetized rats at two to four months after KA or control treatment. Current source density (CSD) analysis (Freeman and Nicholson, 1975; Leung, 1990) was used to reveal the location of synaptic and action currents. Stimulation of CA3 was used to activate the midapical dendrites of CA1 pyramidal cells via Schaffer collaterals (Ishizuka et al., 1990; Li et al., 1994), and stimulation of the medial perforant path (MPP), axons of neurons in the EC, was used to activate the distal dendrites of CA1 pyramidal cells (Leung et al., 1995). The perforant path also activates the CA1 dendrites indirectly through the trisynaptic EC-DG-CA3-CA1 pathway (Fig. 1B) (Andersen et al., 1971; Yeckel and Berger, 1998). The response of CA1 following MPP stimulation is thus an indicator of the neuronal processing through the mono- or multisynaptic EC–hippocampal circuit. We found that excitatory transmission at either basal or distal apical dendrites of CA1 was increased in KA-treated rats as compared with control rats. The increase of both mono- and multisynaptic excitation of the EC to CA1 circuit in KA-treated rats suggests that this circuit may play an important role in increasing seizure susceptibility and in the behavioral deficits induced by seizures. Some results have been presented as an abstract (Wu and Leung, 1996).

EXPERIMENTAL PROCEDURES

Experimental procedures with animals were approved by the University Animal Use Committee. All efforts were made to minimize animal suffering, the number of rats used was near the minimum required to yield statistically significant data, and both DG (Wu and Leung, 2001) and CA1 were studied in the same rat.

KA injection

The procedures have been reported elsewhere (Wu and Leung, 2001). Briefly, male Long-Evans rats (50 to 60 days old) were injected i.c.v. with KA (Sigma, St. Louis, MO, USA) under sodium pentobarbital (60 mg/kg i.p.) anesthesia. KA was injected (0.5 μg in 1-μl volume of artificial cerebrospinal fluid, aCSF) over a 10-min period per side and the needle was left in place for another 2 min after injection. Both unilateral ($N=17$) and bilateral ($N=14$) injections were performed. The seizures were monitored for at least 6 h after injection. Control animals were injected with aCSF or saline. Spontaneous seizures were not monitored systematically for the rats used in this study, but they were found in other rats given the same KA treatment.

Electrophysiology after KA or control treatment

Two to four months after injection, rats were anesthetized with urethane (1.2–1.3 g/kg, i.p.) and positioned in a stereotaxic apparatus. The surgical, stimulation, recording, and analysis procedures were similar to those used in previous reports (Wu et al., 1998; Wu and Leung, 2001). The stimulating and recording electrodes were placed on the same side that KA was injected, whether the injection was unilateral or bilateral. Stimulating electrodes (125-μm Teflon-insulated steel wires) were placed at (1) CA3b: P 3.2, L 3.2 and D 3.6–4.0 mm to directly activate CA1 through the Schaffer collateral system (Fig. 1A); or (2) MPP: P 8, L 4.4, D 3.0–3.3 (D=depth below the skull surface) to activate CA1 directly or indirectly through the classic trisynaptic pathway (Fig. 1B). The depth of the stimulus electrode was optimized by small steps ($\leq$0.1 mm) in order to evoke the largest responses. Photoisolated constant current pulses of 0.2-ms duration were delivered cathodally to one of the two sites at a repetition rate $<$0.15 Hz. A screw in the frontal skull served as the stimulus anode.

Detailed mapping of the field potentials in dorsal hippocampal CA1 (P 3.2–4.0, L 2.2–2.6) was done using a glass micropipette. Preliminary data indicated that mapping of the potential field at 50-μm spatial intervals would sample the field adequately. The micropipette was filled with 2-M sodium acetate and 4% Pontamine Sky Blue (5–15 MΩ) and mounted on a Burleigh Microdrive (Exfo Burleigh Products Group, Victor, NY) (of 1-μm step resolution). The field potentials were amplified, bandpass-filtered between 0.1 Hz (6 dB/octave rolloff to low frequency) and 2 kHz (12 dB/octave rolloff to high frequency) and digitized at 10 kHz. Eight sweeps were averaged using a custom program on a microcomputer. At the stratum (str.) radiatum and cell body layer of CA1, input/output (I/O) profiles were recorded following paired-pulse stimulation of CA3, using various intensities (10–600 μA) and interpulse intervals (IPIs; 10–500 ms). An automated laminar profile of average evoked potentials (AEPs) was then recorded sequentially in a deep-to-surface direction. At one depth, responses to two stimulation sites (CA3 and MPP) were recorded before moving up to the next recording depth. A profile typically spanned 2–2.5 mm from the ventral blade of the DG to the CA1

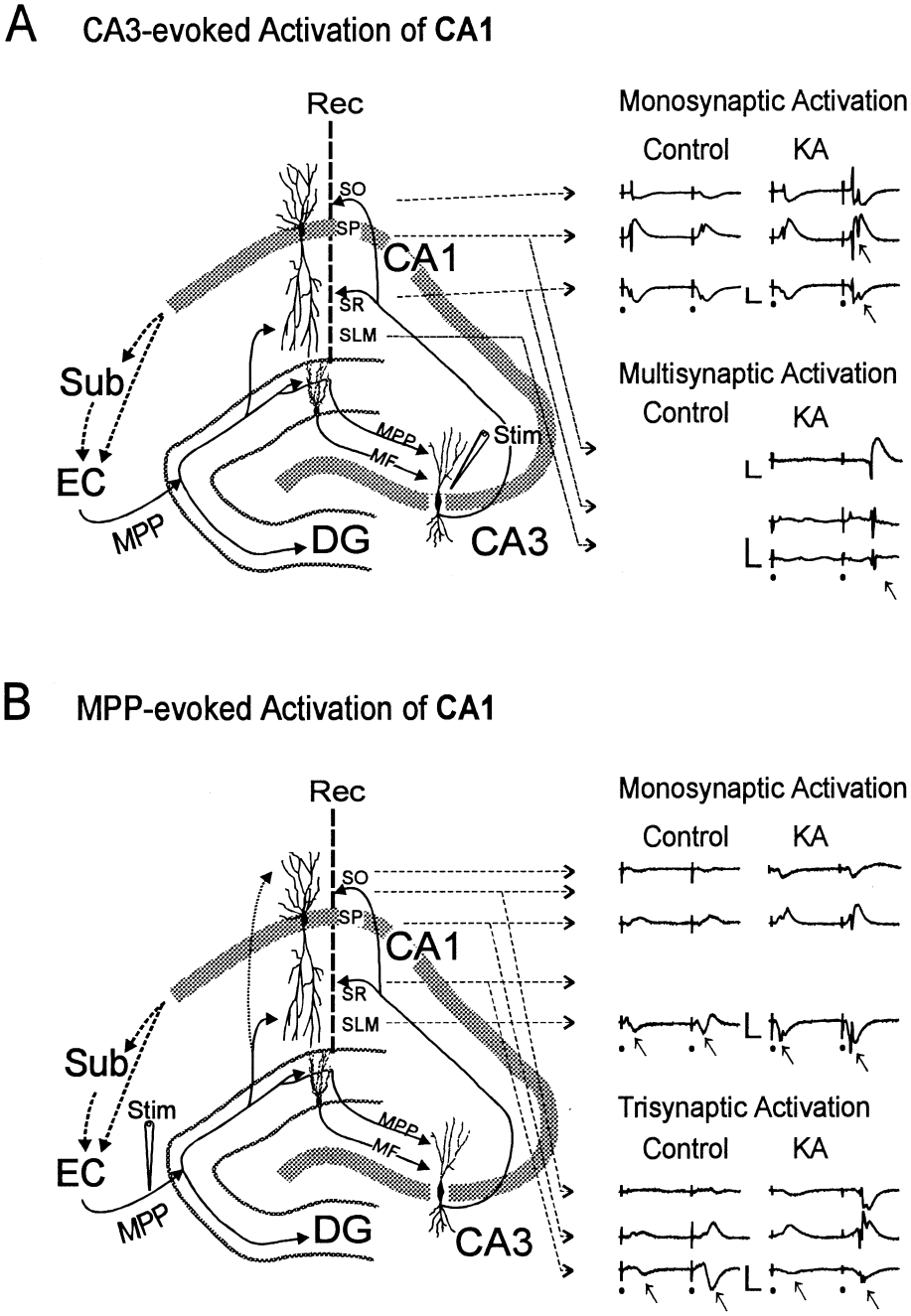

Fig. 1. Schematic drawing showing the stimulating and recording electrode arrangements, neural circuits and the typical CA1 current sinks in control and kainic acid-treated rats. (A) CA3 stimulation (200 μA, 50 ms interpulse interval) evoked monosynaptic excitatory synaptic current sinks in the SO (stratum [str.] oriens) and SR (str. radiatum), resulting in short-latency spikes sink in the SP (str. pyramidale). The spikes showed paired-pulse inhibition in control rats, but paired-pulse facilitation in kainic acid (KA)-treated rats, resulting in spike bursts (arrows). CA3 stimulation also evoked a multisynaptic long-latency population spike at the distal dendrites of CA1 (arrow) via a CA3-CA1-EC-hippocampal loop. (B) Stimulation of medial perforant path (MPP) evoked a monosynaptic excitatory synaptic current sink in the str. lacunosum-moleculare (SLM) and a trisynaptic long-latency current sink in the SR of CA1 (arrows) in both control and KA-treated rats. However, short-latency or long-latency spikes were only observed in KA-treated rats. EC, entorhinal cortex; DG, dentate gyrus; Sub, subiculum; Rec, recording; Stim, stimulation; MF, mossy fibers. The labels are the same in the following figures unless otherwise specified.

alveus and took about 90 min. Recordings at a nonmoving glass electrode in the DG provided an indicator of the response stability.

Alternately, extracellular potentials were recorded simultaneously from 16 channels on a silicon probe (Kloosterman et al., 2001). The silicon probe, fabricated by the NIH Center for Communications Technology, University of Michigan, consisted of 16 electrodes with 100-μm spacing, lined up in a linear array. The silicon probe was lowered to record from the CA1 and the dorsal blade of the DG. Following a high-pass (0.08 Hz) filter, the 16 channels were digitized at 20 kHz following 16 sample-and-hold circuits.

Drug administration

I.c.v. injections included 1.5 μl of 20-mM (30 nmol total) bicuculline methiodine (Sigma), a $GABA_A$ receptor antagonist; 2 μl of 50-mM D-2-amino-5-phosphonopentanoic acid (D-AP5), an *N*-methyl-D-aspartate (NMDA) receptor antagonist; and 2.5 μl of 10-mM 6-cyano-7-nitroquinoxaline-2,3-dione (CNQX), a non-NMDA receptor antagonist. The field potentials were recorded using the 16-channel silicon probe (and CSDs estimated) before and after drug injection.

Data analysis

CSDs were calculated in one (z) dimension, assuming that currents in the x and y directions were negligible, using the formula (Freeman and Nicholson, 1975; Kloosterman et al., 2001; Leung, 1990)

$$\mathrm{CSD}(z) = \left[\frac{[2\phi(z) - \phi(z + 2\Delta z) - \phi(z - 2\Delta z)]}{(2\Delta z)^2}\right]\sigma_z$$

where CSD(z) is the current-source-density at depth z, $\phi(z)$ is the AEP at depth z, Δz is the depth interval (typically 50 μm for glass pipette recording, 100 μm for 16-channel probe recording), σ_z is the conductivity in the z direction, assumed homogeneous. CSDs were calculated in units of mV/mm, and these values of CSD should be multiplied by the conductivity (σ_z) to give actual current densities. The inhomogeneity in layer-by-layer conductivity in the hippocampus of control rats did not alter the major CSDs in the latter rats (Kloosterman et al., 2001; Leung et al., 1995), but conductivity in KA-treated rats has not been measured.

For I/O curve and IPI relationship, the slope of the EPSP was measured at the str. radiatum of CA1 at about 1–1.5-ms window of time (starting 0.2–0.4 ms after EPSP onset, but ending at >0.2 ms before the onset of a population spike [PS]). The amplitude of the PS was measured at CA1 cell layer from the onset to the negative peak of AEP. The paired-pulse ratio (PPR) of the peak amplitude of the PS or EPSP slope was estimated as the ratio of the second to the first response following paired-pulse stimulation. Paired-pulse facilitation (PPF) occurred when PPR>1, while paired-pulse inhibition corresponded to PPR<1. For excitatory current sinks, the latencies of onset (the time that the sink started after stimulation), the half-peak duration (measured as the time that a response took to decay from the peak to half-peak amplitude) and the peak amplitude were measured at the location of the maximal sink at various layers of CA1. For the population spike sinks, the peak latency and the peak amplitude were measured. The PPR of the peak amplitude of current sink and spike was also measured. Analysis of variance (ANOVA; repeated measure of ANOVA followed by Tukey's Protected t-test post-hoc and analysis of covariance [ANCOVA]), a nonparametric Wilcoxon test, χ and paired t-tests were used for estimating statistical significance, assumed to be at the $P<0.05$ level.

Histology

At the end of each experiment, the stimulating electrode positions were marked by a lesion made by passing a direct current of 0.5 mA for 1 s. The recording micropipette was placed sequentially at the str. radiatum and the CA1 cell layer, as estimated by the electrophysiologic responses (Fig. 1A). At each location, dye was ejected from the micropipette by connecting to the cathode of a 48-volt voltage source for 10 min, with the anode of the voltage source connected to a skull screw. Electrode sites of the silicon probes were not directly verified. In order to locate the approximate track of the probe, a glass pipette was lowered in the same track as the probe and dye was ejected at the location of the maximum population spike in CA1. Under deep anesthesia, the animals were transcardially perfused with 1% buffered sodium sulfide solution (pH, 7.4) 100 ml, 1% paraformaldehyde+1.25% glutaraldehyde solution 100 ml (pH 7.4) and followed by 1% buffered sulfide solution (pH 7.4) 100 ml. The brain was removed and postfixed in 1% paraformaldehyde+1.25% glutaraldehyde solution. Coronal sections of 40-μm thickness were cut using a cryostat and stained with Thionin to verify the electrode placement and cell loss.

RESULTS

Histology of KA-treated rats

KA injection resulted in a loss of CA3 cells, particularly from CA3c and CA3b and less so from CA3a (see Fig. 2A of Wu and Leung, 2001). After a unilateral injection, the contralateral CA3 showed variable CA3 cell loss (mostly in CA3c). In thionin-stained sections, the EC appeared intact in both KA-treated and control rats; however, quantified cell counts were not made. Only the side with KA injection was recorded in unilaterally KA-treated animals. The following results were not different between the unilateral and bilateral KA treatment groups, and the results from the two groups were combined.

Enhancement of EPSP/PS coupling in CA1 following KA seizures

Population EPSPs were acquired at str. radiatum of CA1 following paired-pulse stimulation of CA3b at various intensities and IPIs (Fig. 1A). The threshold for evoking a visible EPSP at the str. radiatum of CA1 was 22±1.5 μA (N=32) in control and 16±2.3 μA (N=31) in KA-treated rats, respectively; there was no significant difference in the thresholds of the two groups. However, the EPSP slope following the first stimulus pulse (EPSP1) recorded at str. radiatum of CA1 was significantly different between KA-treated and control rats (Fig. 2A), with the maximal EPSP slope smaller in KA-treated than control rats. The EPSP slope following the second stimulus pulse (EPSP2) was relatively similar between KA-treated and control rats (Fig. 2B). The EPSP2/EPSP1 ratio showed a robust difference between KA-treated and control rats (Fig. 2C); the ratio was smaller at low stimulus intensity (20–60 μA) and larger at high intensity (200–600 μA) in KA-treated rats as compared with control rats (Fig. 2C). At a fixed intensity of 200 μA, the EPSP2/EPSP1 ratio was significantly larger at all IPIs tested (10–500 ms) in the KA-treated group than in the control group (Fig. 2D).

The threshold for evoking a PS, with onset latency of 5–7 ms, in CA1 following CA3b stimulation was 50±5 μA (N=31, range 10–100 μA) in KA-treated rats, which was significantly lower ($P<0.01$) than 85±10 μA threshold (N=32, range 40–200 μA) in control rats. Thus, the PS following the first pulse (PS1) tended to be larger at low stimulus intensities (≤80 μA) in KA-treated than in control rats (Fig. 3A). The PS1 amplitude was significantly smaller in KA-treated than in control rats at >200 μA CA3b stimulation (Fig. 3A).

The most robust change in PS occurred after the second pulse (PS2). PS2 amplitude was significantly larger in KA-treated than in control rats at 80–600 μA (Fig. 3B). Consequently, PS2/PS1 amplitude ratio was

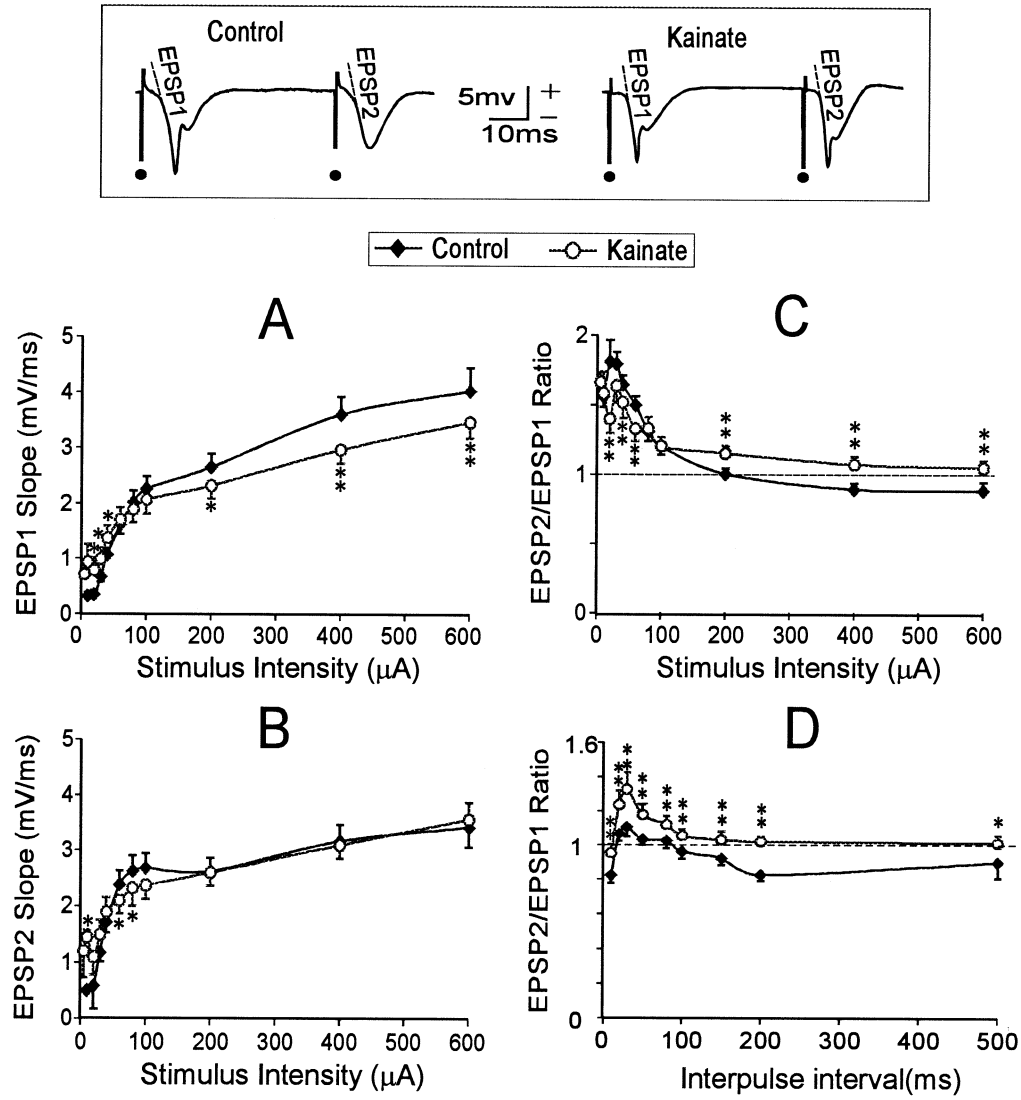

Fig. 2. Increased paired-pulse facilitation (PPF) of CA1 EPSPs in kainic acid (KA)-treated rats. Excitatory postsynaptic potential (EPSP) slope and PPF of population EPSPs recorded at the stratum radiatum of CA1 (inset at top) following various intensities and interpulse intervals (IPIs) of CA3b stimulation. PPF was greater in KA-treated ($N=31$) than in control rats ($N=32$). (A) The relation of the slope following the first stimulus pulse (EPSP1) to stimulus intensity showed a statistically significant difference between the KA-treated and control groups (** $P<0.01$, two-way repeated measure analysis of variance [ANOVA]). Post-hoc test (Tukey's Protected *t*-test) revealed that the EPSP1 slope was significantly larger at 20-40 μA, but smaller at 200–600 μA stimulus intensities in KA-treated than control rats (* $P<0.05$, ** $P<0.01$). (B) Plot of the slope following the second stimulus pulse (EPSP2) against stimulus intensity showed a statistically significant difference between the KA-treated and control groups (* $P<0.05$, two-way repeated measure ANOVA). EPSP2 slope was significantly larger at 30 μA, but smaller at 80- to 100-μA stimulus intensities in KA-treated than control rats (* $P<0.05$, Tukey's Protected *t*-test post-hoc). (C) Paired-pulse ratio (EPSP2/EPSP1) was significantly different between the control and KA-treated groups (** $P<0.01$, two-way repeated measure ANOVA). The EPSP2/EPSP1 ratio was significantly smaller at 20-60 μA, but larger at 200-600 μA intensities in KA-treated than control rats (** $P<0.01$, Tukey's Protected *t*-test post-hoc). (D) Plot of the EPSP2/EPSP1 ratio against IPI showed a significant difference between the control and KA-treated group. EPSP2/EPSP1 ratio was significantly larger in KA-treated than control rats at all IPIs tested (* $P<0.05$, ** $P<0.01$, Tukey's Protected *t*-test post-hoc).

significantly larger in KA-treated than in control rats at 100-600 μA (Fig. 3C). The plot of PS2 amplitude against PS1 amplitude revealed that PS2 was larger in KA-treated than in control rats for a given PS1 (Fig. 3D), suggesting that a larger PPR of PS in KA-treated rats was not due to a smaller PS1 amplitude. The amplitude of PS2 increased with the PS1 amplitude in KA-treated rats (solid regression line in Fig. 3D), but hardly changed with the PS1 amplitude in control rats (dotted regression line in Fig. 3D).

PS2/PS1 amplitude ratio was significantly larger in KA-treated than in control rats at most IPIs tested (Fig. 4C). The paired-pulse inhibition phase of CA1 PSs was found only at <20 ms IPIs in KA-treated rats, as compared with <80 ms IPIs in control rats. Since the difference in PS1 amplitude between KA-treated and control rats was

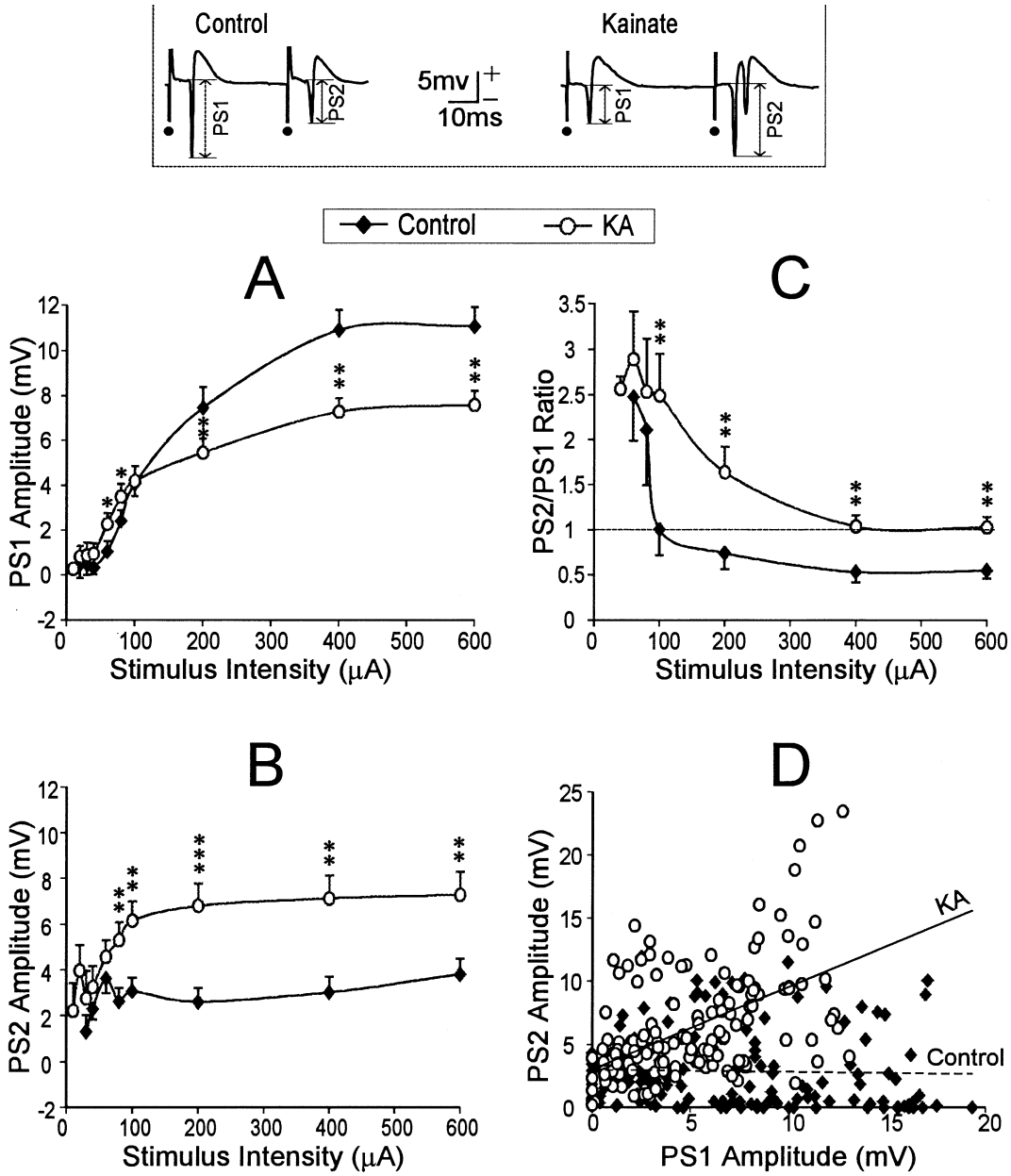

Fig. 3. Paired-pulse facilitation (PPF) of population spikes in CA1 was increased in kainic acid (KA)-treated rats as compared with control rats. PPF of CA1 population spikes (PSs) following CA3 stimulation at various intensities and fixed 50-ms interpulse interval was increased in KA-treated ($N=31$) compared with control rats ($N=32$). Inset at top shows sample recordings from control and KA-treated rats and measurement of PS. (A) The amplitude of the PS following the first pulse (PS1) was significantly different between the control and KA-treated groups (** $P<0.01$, two-way repeated measure analysis of variance [ANOVA]). PS1 amplitude was significantly larger at 60- to 80-μA, but smaller at 200- to 600-μA stimulus intensities in KA-treated than in control rats (* $P<0.05$, ** $P<0.01$, Tukey's Protected *t*-test post-hoc). (B) The amplitude of the PS following the second pulse (PS2) was significantly larger in the KA-treated than in the control group (** $P<0.01$, two-way repeated measure ANOVA). PS2 amplitude was significantly larger at 80-600 μA in KA-treated than in control rats (**$P<0.01$, *** $P<0.005$, Tukey's Protected *t*-test post-hoc). (C) The ratio of PS2 to PS1 amplitudes (PS2/PS1) was significantly different between the control and the KA-treated group (** $P<0.01$, two-way repeated measure ANOVA). At 100- to 600-μA stimulus intensities, PS2/PS1 ratio was significantly larger in KA-treated than in control rats (** $P<0.01$, Tukey's Protected *t*-test post-hoc). (D) The plot of the amplitude of PS2/PS1 showed that the amplitude of PS2 increased with PS1 amplitude in the KA-treated group, while PS2 amplitude slowly decreased with PS1 amplitude in the control group. For the KA-treated group, the regression line is $y=3.1+0.64x$, while for the control group, $y=3.1-0.02x$, where y=PS2 amplitude and x=PS1 amplitude.

small at 200 μA CA3 stimulation, the difference in PS2/PS1 amplitude ratio was mainly attributed to the difference in PS2 amplitudes between the KA-treated and control groups of rats (Fig. 4A, B).

Spike generation from the EPSP was analyzed by plotting the amplitude of population spike at the cell layer against EPSP slope at str. radiatum of CA1. There was a left or upward shift of PS–EPSP curve in the KA-treated as

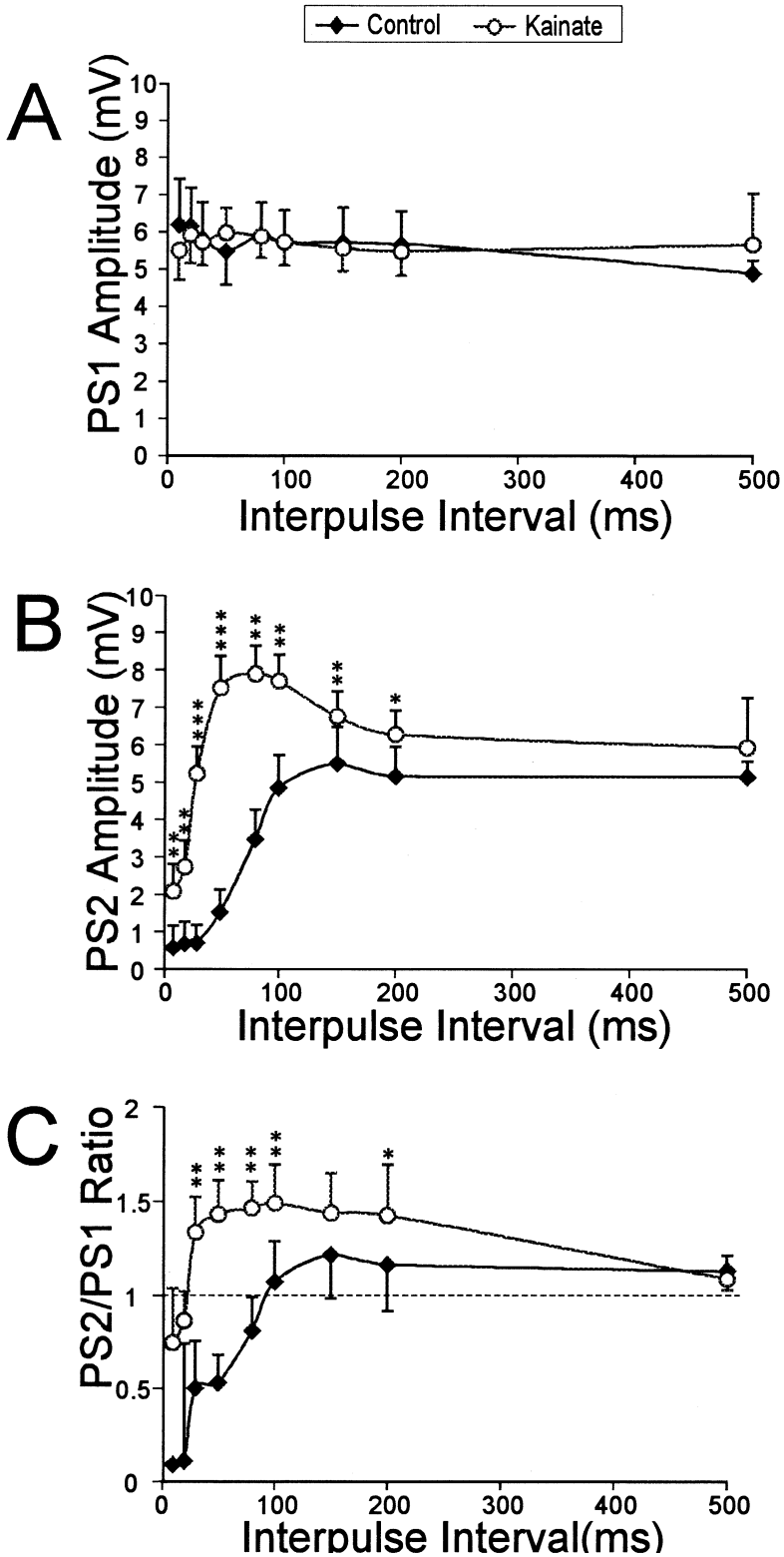

Fig. 4. Paired-pulse facilitation (PPF) of population spikes (PSs) in CA1 in kainic acid (KA)-treated rats was increased at 10- to 200-ms interpulse intervals (IPIs). PPF of CA1 PSs following CA3 stimulation at various IPIs (fixed 200-μA intensity) was greater in KA-treated (N=25) than in control rats (N=26). (A) The amplitude of PS1 was not statistically different between control and KA-treated groups. (B) The amplitude of PS2 was statistically different between control and KA-treated groups (** $P<0.01$, two-way repeated measure analysis of variance [ANOVA]). PS2 amplitude was significantly larger in KA-treated than in control rats at 10-200 ms of IPIs (* $P<0.05$, ** $P<0.01$, Tukey's Protected t-test post-hoc). (C) PS2/PS1 ratio was significantly different between control and KA-treated groups (**$P<0.01$, two-way repeated measure ANOVA). PS2/PS1 ratio was significantly increased at IPIs of 30-200 ms (except 150 ms) in KA-treated as compared with control rats (* $P<0.05$, ** $P<0.01$, Tukey's Protected t-test post-hoc).

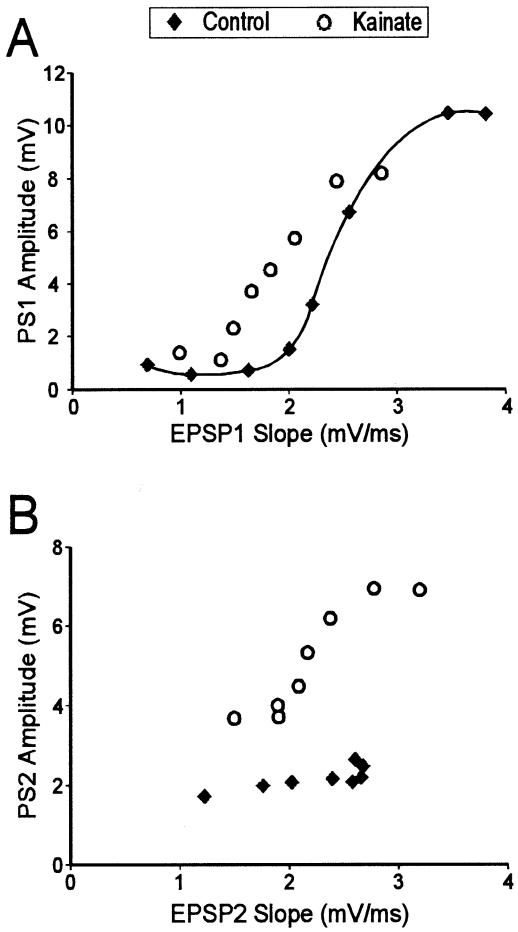

Fig. 5. Excitatory postsynaptic potential (EPSP)-spike coupling in CA1 was increased in kainic acid (KA)-treated as compared with control rats. Population spike (PS) amplitude was plotted as a function of EPSP slope using CA3 stimuli of various intensities but fixed 50-ms IPI. (A) An S-shaped curve was found for the amplitude of PS following the first pulse vs EPSP slope following the first stimulus pulse in control and KA-treated rats, with the curve significantly shifted left in KA-treated as compared with control rats ($P<0.01$, analysis of covariance [ANCOVA]). (B) For the amplitude plot of EPSP slope following the first stimulus pulse/PS following the second pulse, the curve for KA-treated rats was significantly above that for control rats ($P<0.001$, ANCOVA).

compared with control rats, suggesting an enhanced EPSP to spike (E–S) coupling (Fig. 5). For EPSP1≥ 1.5mV/ms or EPSP2≥2mV/ms, the amplitude of PS (PS1 or PS2) was significantly larger in KA-treated than control group (Fig. 5, $P<0.01–0.001$, ANCOVA).

Increased PPF of monosynaptic excitatory dendritic sinks in CA1 following CA3 stimulation in KA-treated rats

Laminar profiles of field potentials in CA1 were mapped by a micropipette following paired-pulse stimulation of CA3b at 50 ms IPI and 200 μA, which was an intensity that evoked 60–75% of the maximal PS1 amplitude. In control rats, CA3b stimulation evoked negative waves at apical and basal dendrites (line filled areas at SR and SO, respectively, in Fig. 6A) accompanied by a positive wave at the cell layer. Consistent with a previous study (Roth and Leung, 1995), CSD analysis revealed that the negative wave at the basal dendrites corresponded to a sink at str. oriens (vertical line-filled areas in Fig. 6C), while the apical dendritic negative wave corresponded to a sink at str. radiatum (slanted line-filled areas in Fig. 6C), and the cell layer served as a source. Thus, it has been inferred that ipsilateral CA3b stimulation provided excitation to both the basal and apical dendrites of CA1 (Roth and Leung, 1995), but the peak excitation was significantly larger at the apical dendrites (str. radiatum) than basal dendrites (str. oriens) in control rats (Table 1, $P<0.001$, paired *t*-test).

The basal dendritic sink in CA1 following paired-pulse, but not single-pulse, CA3b stimulation was increased in KA-treated as compared with control rats (Table 1). In contrast, the apical dendritic (str. radiatum) sink was smaller, although not statistically significantly, in KA-treated as compared with control rats (Table 1). The PPF of the peak sink amplitude in both str. oriens and radiatum following paired-pulse CA3b stimulation was significantly larger in the KA-treated than in the control group (Table 1). KA-treated rats also showed a more prolonged EPSP sink as compared with control rats. The half-peak duration of the str. oriens sink was significantly longer for KA-treated than control rats, after either the first or the second pulse, while the half-peak duration of the str. radiatum sink was significantly longer for KA-treated than control rats only after the second pulse (Table 2).

Enhancement of CA1dendritic spikes following CA3 stimulation in KA-treated rats

In control rats, CA3b stimulation of moderate intensity (200 μA) resulted in a PS in CA1 (AEP profiles in Fig. 6A). CSD analysis showed that the sharp spike sink started at the proximal apical dendrites and propagated to the cell body layer of CA1 (star in Fig. 6C, E). The earliest spike sink was found at the proximal apical dendrites in all rats (Kloosterman et al., 2001), about 100–150 μm (130±6 μm, $N=32$) below the cell body layer (arrows in Fig. 6C, E). The peak latency of the PS was 7.1±0.3 ms ($N=32$) at the proximal apical dendrites, which preceded the peak PS latency of 7.9±0.3 ms at the CA1 cell layer. The propagation velocity of the population spike over the proximal apical dendrites was about 0.17 mm/ms.

In most KA-treated rats (74%, or 23 of 31 rats), CA3b stimulation evoked a CA1 PS that had the earliest latency at the proximal apical dendrites (Fig. 7A), 119±6 μm ($N=23$) away from the cell body layer. This location of the presumed origin of the population spike in KA-treated rats was not different from that in control rats. However, population spikes in KA-treated rats appeared to propagate further into the distal parts of str. radiatum (Fig. 7A, C). Invasion of the population spike (following CA3b stimulation) into the distal dendritic tree ≥200 μm from the CA1 cell layer (Fig. 7A, E; Fig. 8A) was found in 71% of KA-treated rats as compared with 25% of control rats ($\chi(1)=11.7$, $P<0.01$). In addition, a burst of PSs (≥2 spikes) was found following the second pulse of paired-

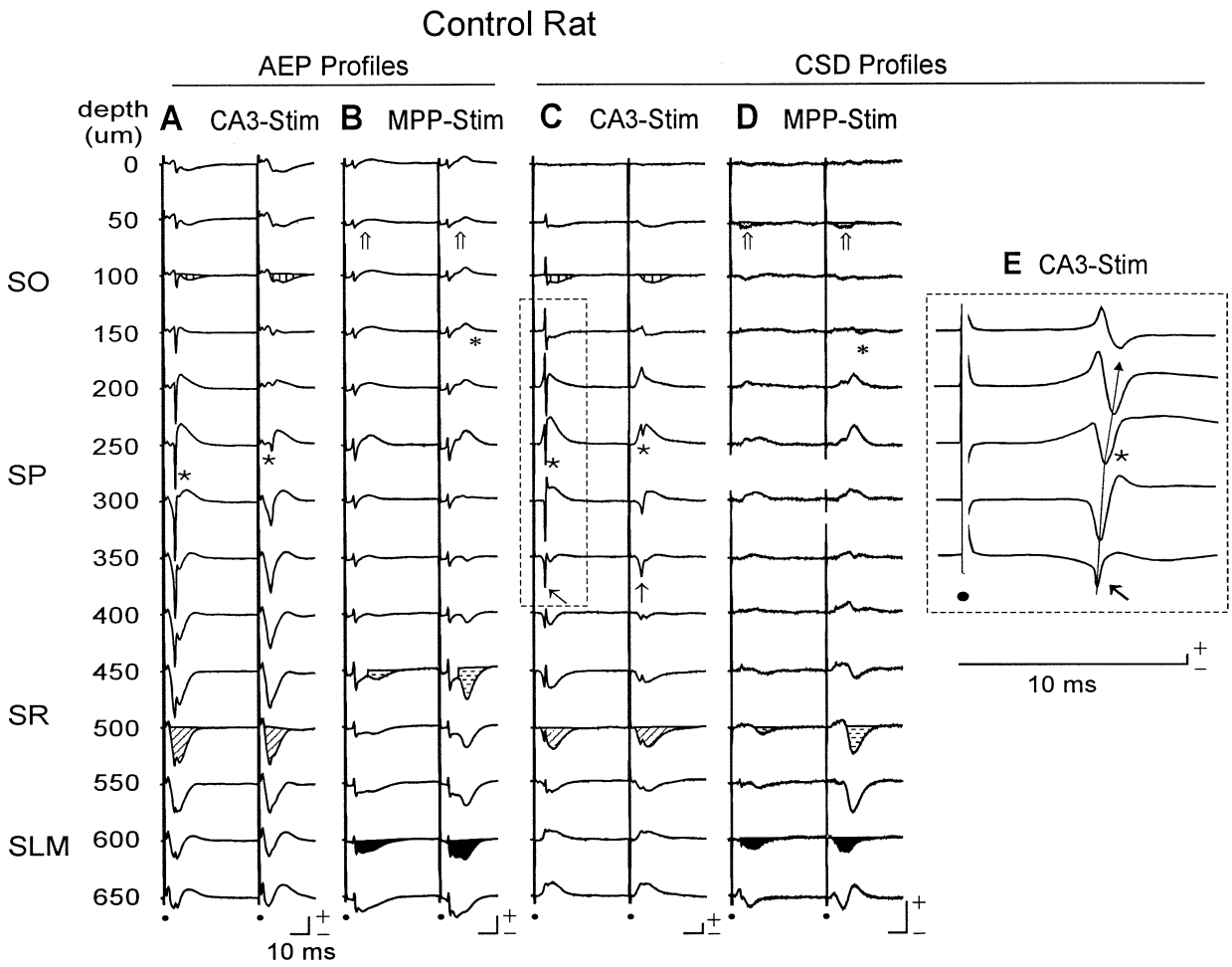

Fig. 6. Laminar profiles of the average field potentials and current source densities (CSDs) in CA1 after CA3 and medial perforant path (MPP) stimulation in a control rat. Laminar profiles of average evoked potentials (AEP) in CA1 of a representative control rat (MFA125) mapped at 50-μm depth intervals (A, B) and the corresponding CSD time transients (C, D and E). Paired-pulse (200-μA, 50-ms interpulse interval) stimulation was delivered to CA3 (A, C, E) or MPP (B, D). (A, C and E) Following CA3 stimulation, stars indicate population spikes in the CA1 cell layer, and arrows in C and E indicate the spike with the earliest peak latency at proximal apical dendrites of CA1. Vertical and slanted line-filled areas indicate the maximum negative potentials or current sinks in the stratum (str.) oriens (SO) and str. radiatum (SR), respectively. (B and D) Following MPP stimulation, black-filled areas indicate early latency negative potentials or current sinks in the stratum lacunosum-moleculare (SLM). Horizontal dotted line-filled areas indicate late latency negative potentials or sinks in the str. radiatum. Vertical line-filled area and/or star indicates a small late sink in the str. oriens. Hollow arrows and shaded areas with open arrows indicate field potentials and early current sinks in the str. oriens. (E) The traces in dotted box in C were shown in a larger time scale. Line with arrowhead indicates the direction of spike propagation. Dots indicate stimulation artifacts. Scale bars in A and B are 5 mV and 10 ms. Scale bars in C, D and E are 500 mV/mm^2 and 10 ms. Positive or source is up.

pulse CA3 stimulation in 65% (20 of 31) of KA-treated rats (Fig. 8A), but in no (0 of 32) control rats.

In 26% (8 of 31) of the KA-treated rats, CA3b stimulation evoked a population spike sink that showed the earliest latency at the proximal *basal* dendrites (hollow arrow in Fig. 7E), and then propagated to the cell body and apical dendrites (Fig. 7E). The onset latency of the basal dendritic spike varied from 5-8 ms (three rats) to >10 ms (five rats),

Table 1. Increased stratum oriens but not stratum radiatum EPSP sink in KA-treated than in control rats following paired-pulse stimulation of CA3 (200 μA, 50 ms interpulse interval, IPI)

Sink site	Treatment (*N*)	Peak sink EPSP1 (mV/mm^2)	Peak sink EPSP2 (mV/mm^2)	EPSP2/EPSP1
Stratum	Control (32)	327±25	350±20	1.2±0.2
Oriens	KA (31)	314±30	469±37*†	1.6±0.1*
Stratum	Control (32)	556±51	542±43	1.0±0.05
Radiatum	KA (31)	427±48	486±41	1.3±0.1*

* $P<0.01$, as compared to control group.
† $P<0.01$, as compared to corresponding pulse 1 (non-parametric Wilcoxon test).

Table 2. Increased duration of EPSP sink at CA1 stratum oriens and stratum radiatum in KA-treated as compared to control rats following paired-pulse CA3 stimulation (200 μA, 50 ms IPI)

Sink site	Treatment (*N*)	Onset latency (ms)		Peak latency (ms)		Half-peak duration (ms)	
		Pulse 1	Pulse 2	Pulse 1	Pulse 2	Pulse 1	Pulse 2
Stratum	Control (32)	5.8±0.4	5.6±0.4	11.9±0.4	11.9±0.5	15.8±0.4	16.7±0.4
Oriens	KA (31)	5.4±0.4	5.1±0.4	12.8±0.6	13.2±0.5	17.6±0.7*	19.0±0.6**
Stratum	Control (32)	4.6±0.2	4.1±0.2	10.6±0.3	10.2±0.3	14.8±0.4	14.9±0.3
Radiatum	KA (31)	5.0±0.8	4.3±0.4	11.2±0.7	10.8±0.6	15.7±0.7	16.2±0.7*

* $P<0.05$, ** $P<0.01$, as compared to control group (non-parametric Wilcoxon test).

suggesting that the spike may arise from mono- or polysynaptic excitation of the basal dendrites. No CA1 PS with a proximal basal dendritic origin was found following CA3b stimulation in control rats.

Enhancement of the monosynaptic distal apical dendritic current sink in CA1 following MPP stimulation in KA-treated rats

MPP stimulation evoked a short-latency synaptic excitation of the distal dendrites of CA1 pyramidal cells. In control rats, the latter was manifested as a negative wave in the distal apical dendrites (Fig. 6B). CSD analysis revealed an SLM sink of 2–4 ms onset latency (black-filled area, Fig. 6D) accompanied by a source at str. radiatum. The second pulse of a paired-pulse stimulation of MPP always evoked a larger SLM sink than the first pulse (Leung et al., 1995). The SLM sink in response to paired pulses was significantly larger in KA-treated than in control rats, although the first-pulse response was not significantly different between the two groups (Table 3). The onset and peak latencies or half-peak duration of the SLM sink were not statistically different between the control and KA-treated rats (data not shown).

A short-latency (<10 ms) PS in CA1 was not found in control rats after MPP stimulation (200 μA), as reported before (Leung et al., 1995). In contrast, a short latency (4–6 ms) PS in CA1 following MPP stimulation was found in 65% (20 of 31) of KA-treated rats. The spike followed the early (2–4-ms onset) MPP-evoked distal apical dendritic excitation (SLM sink; black-filled areas in Fig. 7B, F). In most KA-treated (15 of 20) rats with a PS, an active spike sink was found in the middle or distal apical dendrites, >200 μm from the cell body layer (X in Fig. 7B, F). In eight of 15 rats, the distal apical dendritic spike seemed to follow a proximal apical dendritic or cell layer spike (Fig. 8B). In seven of 15 rats, the spike appeared to start at the mid-distal apical dendrites and propagated to the proximal parts of apical dendrites (arrowhead in Fig. 7B, white arrows in Fig. 7D).

MPP stimulation also evoked an early latency (2.5–5 ms) sink in the distal basal dendrites of CA1 in some control (five of 25) and KA-treated (eight of 22) rats (shaded areas with hollow arrows in Fig. 6D, 7B). The early distal basal dendritic sink was small (<100 mV/mm) and not significantly different between KA-treated and control groups.

Changes in trisynaptic excitation in CA1 following MPP stimulation in KA-treated rats

MPP stimulation evoked a late negative wave of ≥9 ms onset latency in the apical dendrites (Fig. 1B), which corresponded to a sink at in the str. radiatum accompanied by a large source in the stratum pyramidale (SP) and a small source in the distal SLM (slanted line-filled areas in Fig. 6B). As shown in previous studies (Andersen et al., 1971; Leung et al., 1995; Yeckel and Berger, 1998), the properties of this late CA1 sink corresponded to a trisynaptic excitation of CA1 following MPP stimulation. The peak amplitude of the late str. radiatum sink was significantly smaller in KA-treated than control rats following the second, but not the first, pulse of a paired-pulse stimulation of MPP (Table 3). The ratio of the peak amplitude of the late str. radiatum sink was also statistically smaller in KA-treated than control rats (Table 3). MPP stimulation also evoked a late sink (≥9 ms) in the basal dendrites of CA1 in control and KA-treated rats (hollow arrow in Fig. 6D, 7B). The peak amplitude of late str. oriens sink was significantly larger in KA-treated than control rats following the second, but not the first, pulse of paired-pulse stimulation of MPP (Table 3).

In control rats, MPP stimulation (≤600 μA of stimulus intensity) did not evoke a trisynaptic (>9 ms) PS in CA1. In KA-treated rats, the second pulse of a paired-pulse MPP stimulation (200 μA) resulted in a late (>9 ms) PS in CA1 in 32% (10 of 31) of the rats (data not shown).

Polysynaptic PS sinks in CA1 following CA3 stimulation in KA-treated rats

In addition to the early-latency PSs, the second pulse of paired-pulse CA3 stimulation evoked long-latency (>10 ms) PSs in CA1 in 32% (10 of 31) of KA-treated (Fig. 7E), but 0% (0 of 32) of control rats. The late PS appeared to start at the proximal str. oriens in CA1 (not shown) at 11-15 ms (five rats) and ≥20 ms (five rats). Three KA-treated rats clearly showed a late PS sink (≥20 ms of onset latency) at the distal apical dendrites ("late" and X in Fig. 7E), in addition to an early PS in the CA1 cell layer (star in Fig. 7E).

Bicuculline-induced paroxysmal activity that depended on NMDA and non-NMDA receptors

In both control ($N=6$) and KA-treated ($N=5$) rats, i.c.v. bicuculline induced PS bursts following CA3 stimulation

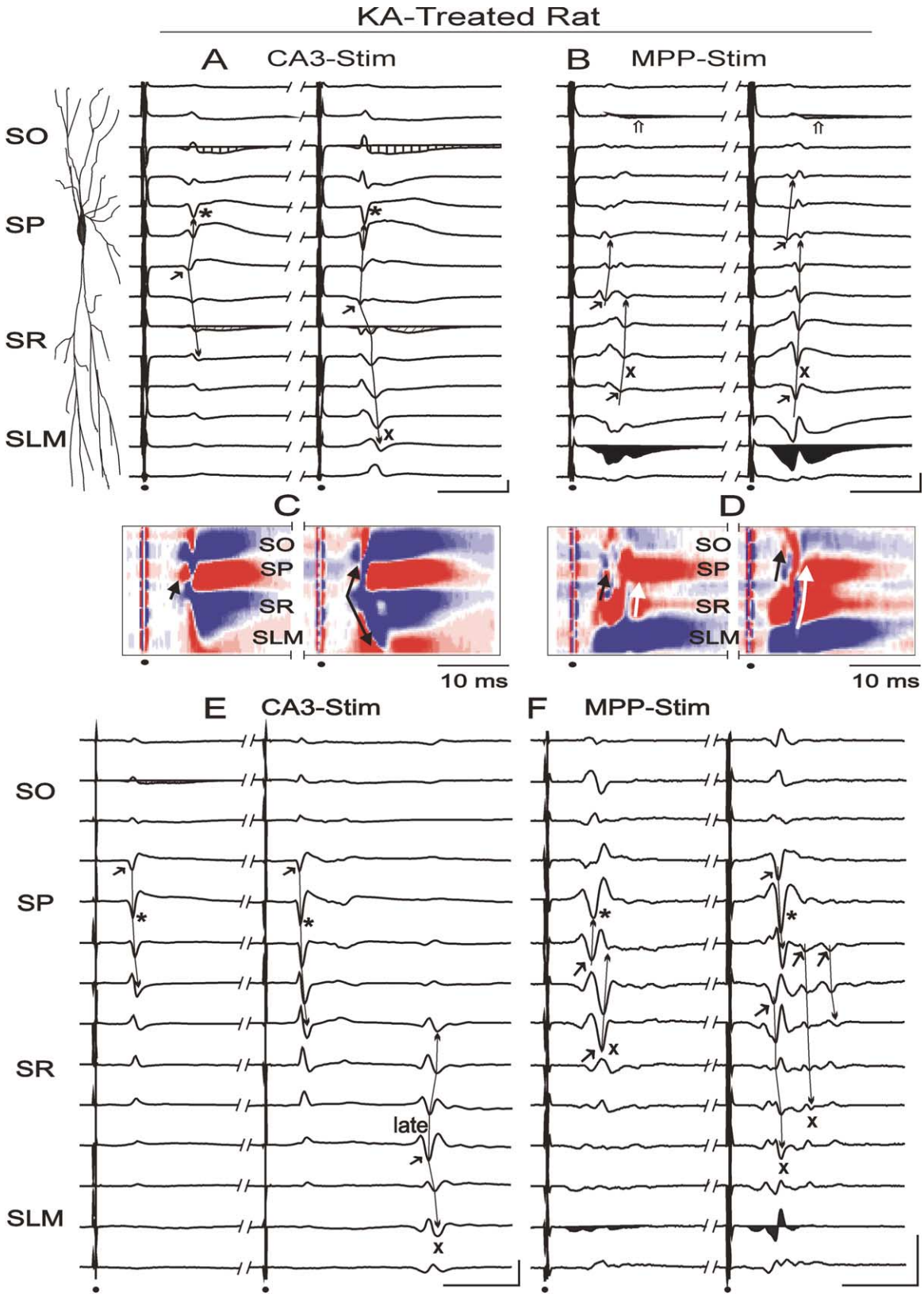

Fig. 7. *(Caption overleaf).*

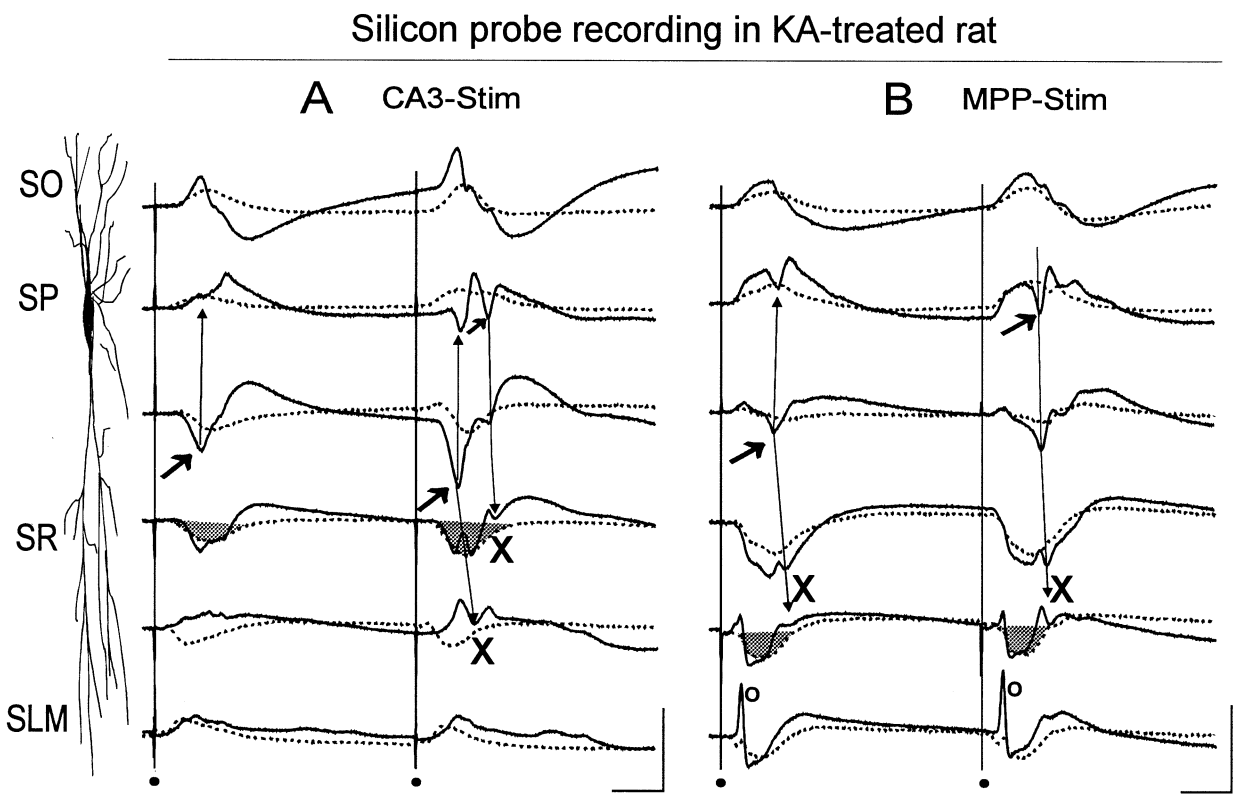

Fig. 8. Dendritic spikes invaded apical dendrites of CA1 in a kainic acid (KA)-treated rat as recorded simultaneously by a silicon probe. Current source densities (CSDs) in CA1 of a KA-treated rat following CA3 (A) or medial perforant path (MPP) (B) stimulation, derived from average evoked potentials (AEPs) simultaneously recorded by a 16-channel silicon probe (100-μm spatial intervals). (A) Dotted line traces show CSDs of excitatory postsynaptic potentials (EPSPs) without population spikes (PSs) after low-intensity (20 μA, 50-ms interpulse interval [IPI]) CA3b stimulation; the maximal sink (shaded gray) is shown in stratum (str.) radiatum. Solid line traces evoked by moderate stimulus intensity (200 μA) show the onset of the PS at the proximal apical dendrites (arrow) or cell layer, and subsequent propagation (line with arrowhead) to the distal apical dendrites. PS at distal apical dendrites labeled with cross (X). (B) Following MPP stimulation of low intensity, dotted lines indicate early EPSP sink (shaded gray for maximal sink after first pulse) at stratum lacunosum-moleculare and str. radiatum, while PS appears to start at the proximal apical dendrites or cell layer in this rat, and then invade the distal str. radiatum (X). Open circle indicates artifact corresponding to the source of dentate PS that invaded into CA1 because the relatively large CSD spatial interval (100 μm). Scale bars are 500 mV/mm^2 and 10 ms. (MFA129). Source is up.

and increased the duration of the sink at str. radiatum (Fig. 9A, B). The amplitude of the first spike in PS bursts and the duration of the str. radiatum sink after bicuculline in KA-treated rats were larger than the respective measures in control rats ($P<0.05$). The combination of glutamate ionotropic antagonists, CNQX and D-AP5, abolished PS bursts and decreased the peak str. radiatum sink in CA1 of control rats by 94±4.8% (Fig. 9A, $N=4$). In KA-treated rats, the combination of CNQX and D-AP5 decreased the peak str. radiatum sink by 24±7.6% (Fig. 9B; $N=4$), significantly less than in control rats ($P<0.05$, Wilcoxon). Typically, an early PS was still observed in KA-treated (but not control) rats after administration of i.c.v. bicuculline followed by CNQX and D-AP5 (star in Fig. 9B, D). CNQX alone (not shown) suppressed the responses almost as well as the combination of CNQX and D-AP5. D-AP5 alone ($N=2$ in

Fig. 7. Current source density (CSD) shows that population spikes (PSs) in CA1 often involved the mid and distal apical dendrites in KA-treated rats. (A, B) A representative rat (MFA42) shows PS following paired-pulse (200 μA, 50-ms interpulse interval [IPI]) stimulation of CA3 (A) and medial perforant path (MPP) (B). (A) Excitatory postsynaptic potential (EPSP) current sinks in the stratum (str.) oriens (SO) and str. radiatum (SR) are illustrated by areas filled with vertical and slanted lines, respectively. The shortest latency of the PS is seen at the proximal apical dendrites (arrow). The PS then propagated proximally to near the cell layer (str. pyramidale [SP]), indicated by a star, or distally to str. radiatum or stratum lacunosum-moleculare (SLM); distal apical spike sink indicated by a cross (X). (B) Short-latency EPSP sink filled with black in SLM. Shaded areas with hollow arrows in indicate the early sink in the str. oriens. PS following SLM excitation appears to start at the distal dendrites (X) and propagate to the cell layer, but a smaller, earlier, proximal apical dendritic spike (onset in str. radiatum) is also shown. (C) CSD contour plot (blue is sink, and red is source) corresponding to (A). The slow EPSP sinks in the str. oriens and str. radiatum (blue areas) accompany the source in SP (red area). Spike propagation is indicated by the arrow along a blue strip. (D) CSD contour plot of (B) reveals the large PS after each pulse started at the distal apical dendrites and propagated toward the cell layer (white arrows), while the smaller, earlier spike started at the proximal apical dendrites (black arrows). (E and F) CSD time transients of another KA-treated rat (MFA25) following paired-pulse (200 μA, 50-ms IPI) stimulation of CA3. Notations same as before. (E) Following CA3 stimulation, a PS started at the proximal basal dendrites and propagated to the apical dendrites. The second pulse evoked a late PS that started at distal str. radiatum. (F) Following MPP stimulation, PSs apparently started at various parts of the proximal dendrites. All parts of figure: Dots indicate the stimulation artifacts. Scale bars are 500 mV/mm^2 and 10 ms. Source is up.

Table 3. The peak amplitude and the paired-pulse ratio of the early stratum lacunosum-moleculare (SLM) sink and the late (≥9 ms onset) sinks in stratum oriens or stratum radiatum of CA1 following MPP stimulation (200 μA, 50 ms IPI) in control and KA-treated rats

Sink site	Treatment (*N*)	EPSP1 (mV/mm^2)	EPSP2 (mV/mm^2)	EPSP2/EPSP1
Early SLM	Control (32)	174±15	239±20$^{\#}$	1.4±0.06
	KA (31)	221±21	337±29$^{**\#}$	1.6±0.05*
Stratum	Control (21)	72±7	99±8$^{\#}$ (26)	1.6±0.2
Oriens	KA (18)	81±7	168±23$^{*\#}$ (21)	2.3±0.3*
Stratum	Control (30)	115±14	390±36$^{\#\#}$ (32)	4.1±0.4
Radiatum	KA (20)	103±10	229±28$^{**\#\#}$ (22)	2.4±0.4**

* $P<0.05$, ** $P<0.01$, as compared to control. $^{\#}$ $P<0.05$, $^{\#\#}$ $P<0.01$, as compared to corresponding pulse 1. A non-parametric Wilcoxon test was used. Bracketed value (*N*) under "Treatment" refers to number of rats for EPSP1 and (EPSP2/EPSP1) ratio; some rats showed EPSP2 but not EPSP1.

control and KA-treated rats) decreased the duration of the long str. radiatum sink after bicuculline (Fig. 9C, D), suggesting that the late str. radiatum sink was mediated partly by NMDA receptors. However, in both control and KA-treated rats, the number of early PS bursts (arrow in Fig. 9C, D) was increased and the late paroxysmal discharges (hollow arrow in Fig. 9C, D) were abolished by D-AP5.

DISCUSSION

We found that after 2–4 months of KA treatment, the basal and distal apical EPSPs were enhanced in CA1 following stimulation of CA3 and MPP. Membrane excitability, in particular following paired-pulse stimulation, was enhanced in KA-treated rats as compared with control rats. The spike enhancement resulted from an increase in E-S coupling and an increase second-pulse EPSP. The PSs originated from and actively invaded the distal apical dendrites (>200 μm from the cell layer) more often in KA-treated than control rats.

Excitation increase and inferred inhibition loss after KA treatment

CSD analysis in this study has distinguished excitatory currents at three different locations on the dendritic tree of CA1 pyramidal cells: basal–dendritic, midapical–dendritic and distal–apical–dendritic. At each dendritic site, an afferent stimulus evoked a current sink of 15–30-ms duration that could be accompanied by PS (and unitary spikes) and blocked by CNQX and D-AP5 (Fig. 9). Thus, we infer that the dendritic current sink corresponds to macroscopic (population) excitatory synaptic currents. In KA-treated rats as compared with control rats, monosynaptic excitation of CA1 (after CA3b stimulation) at str. radiatum (midapical dendrites) was marginally decreased (Table 1; Fig. 2), while trisynaptic excitation at str. radiatum after MPP stimulation was significantly decreased (Table 3). We, and others (see Introduction), did not find evidence of an increased CA1 inhibition after KA treatment, and the decrease in the CA3 to CA1 excitation at str. radiatum is readily explained by the degeneration of CA3 pyramidal cells. In this study, as in other studies (Esclapez et al., 1999; Nadler et al., 1980), KA treatment resulted in loss of CA3c and CA3b cells more than CA3a cells (see Fig. 2A of Wu and Leung, 2001). Since CA3c cells project preferentially to the apical dendrites, while CA3a cells project preferentially to the basal dendrites (Ishizuka et al., 1990; Li et al., 1994), a decrease in str. radiatum excitation is to be expected.

Increase in paired-pulse current sinks was found at the distal apical dendrites and basal dendrites of CA1 in KA-treated as compared with control rats (Tables 1 and 3). Basal dendritic (str. oriens) excitation following CA3b stimulation was relatively small in the control rats (Roth and Leung, 1995), although CA3a stimulation evoked large str. oriens sinks accompanied by PSs (Kloosterman et al., 2001), suggesting that the str. oriens sink was generated by excitatory postsynaptic currents. The latter sink evoked by CA3b stimulation was greatly increased in KA-treated rats (Fig. 6, 7; Table 1), such that the peak sinks at str. oriens and str. radiatum were of comparable amplitudes. Several factors may contribute to the enhancement of basal dendritic excitatory transmission in CA1. First, the latter synapses show robust LTP *in vivo* (Kaibara and Leung, 1993; Roth and Leung, 1995), and seizure activity may induce a similar LTP. Second, recurrent excitation among CA3a/b pyramidal cells, which project heavily to the basal dendrites of CA1 (Ishizuka et al., 1990; Li et al., 1994), would contribute to the increase in polysynaptic CA3 to CA1 basal dendritic excitation (Roth and Leung, 1995). Third, axon collateral sprouting of CA1 pyramidal cells after KA treatment was found preferentially in str. oriens (Esclapez et al., 1999; Perez et al., 1996), suggesting that stronger recurrent (polysynaptic) excitation may occur at the basal dendrites of CA1.

The distal apical dendritic excitation of CA1 following MPP stimulation was enhanced in KA-treated rats, as compared with control rats (Table 3). A short-latency (<9 ms) PS could be evoked by MPP stimulation in CA1 in 65% of KA-treated rats (Fig. 7B), but not in control (0%) rats (Leung et al., 1995). Thus, direct EC control of CA1 was increased following KA treatment.

Enhanced excitation was also revealed when inhibitory $GABA_A$ receptors were blocked by bicuculline. Bicuculline increased the duration of the str. radiatum sink, more in KA-treated than in control rats. One possible mechanism for the prolonged radiatum sink is that bicuculline induced disinhibition of CA3 cells (Wong and Traub, 1983), which recurrently excited each other, and then projected to CA1. The duration of the radiatum sink may reflect a prolonged polysynaptic excitation from CA3 and possibly activation of NMDA receptor currents in CA1. In the KA-treated rats, the

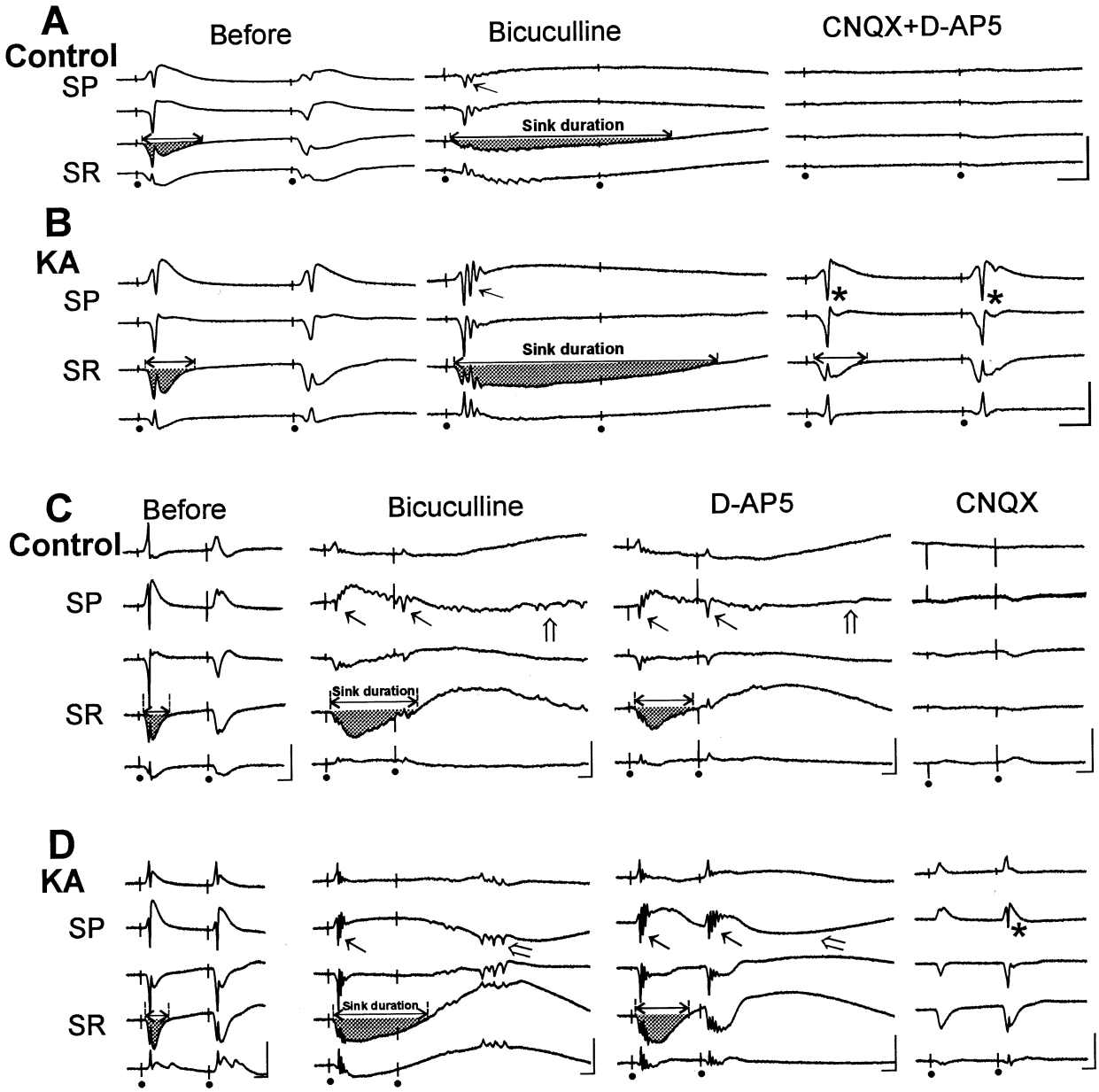

Fig. 9. Kainic acid (KA)-treated and control rats responded differently to $GABA_A$ and glutamate receptor antagonists. (A–D) Current source density (CSD) profiles were derived from simultaneous recordings in CA1 using a 16-channel silicon probe. Bicuculline (1.5 μl of 20-mM bicuculline methoiodide i.c.v.) induced spike bursts (arrows) and increased sink duration in CA1 (first-pulse excitatory postsynaptic potential [EPSP] sink in the stratum (str.) radiatum shaded in gray) in both control (A) and KA-treated rat (B). The sink duration was longer and spike bursts were larger after bicuculline in the KA-treated (B) than the control rat (A), and a mixture of 6-cyano-7-nitroquinoxaline-2,3-dione (CNQX) and D-2-amino-5-phosphonopentanoic acid (D-AP5) (i.c.v.) suppressed the responses almost completely in the control rat (A), but only partially in the KA-treated rat (B). (C) In another control rat, D-AP5 alone blocked the bicuculline-induced late discharges (hollow arrows), but not the early responses (solid arrows), while adding CNQX blocked the early responses as well. (D) In another KA-treated rat, D-AP5 alone also blocked the late paroxysmal discharges (open arrows) but it enhanced the early spike bursts (solid arrows); subsequent CNQX abolished the bursting but a single population spike remained after the second pulse. Dots indicate the stimulation artifacts. Scale bars are 500 mV/mm^2 and 10 ms. Source is up.

excitatory sinks following bicuculline administration were not completely blocked by CNQX and D-APV (Fig. 9). We suggest that synaptic activations in KA-treated (but not control) rats released high concentrations of glutamate that competed favorably with the competitive antagonists (CNQX and D-APV) for binding to the non-NMDA or NMDA receptors. Alteration of antagonist efficacy is possible, but we have no evidence of this. The spike bursts were blocked by non-NMDA and NMDA receptor antagonists, consistent with previous *in vitro* studies (Bernard and Wheal, 1995; Simpson et al., 1991; Turner and Wheal, 1991).

The increase of the second-pulse rather than the first-pulse excitation in KA-treated rats as compared with control rats may suggest presynaptic and postsynaptic mech-

anisms. Presynaptic facilitation through residual Ca (Wu and Saggau, 1997; Zucker, 1989) and enhancement of glutamate release would increase the PPF of the EPSPs in CA1 as reported following kindling *in vitro* (Zhao and Leung, 1991). A decrease in postsynaptic dendritic inhibition would remove inhibitory shunting and increase the amplitude and duration of an EPSP. Dendritic inhibition may be impaired as a result of a loss in excitation to the inhibitory interneurons (Bekenstein and Lothman, 1993; Hirsch et al., 1999), or a loss of selective interneurons that project to the dendrites (Best et al., 1993; Best et al., 1994; Freund and Buzsaki, 1996; Morin et al., 1999). Dendritic but not somatic inhibition was inferred to decrease *in vitro* following experimental epilepsy (Cossart et al., 2001).

We inferred a loss of inhibition in the KA-treated rats in this study, based on several observations. For a given EPSP, we showed an original result (see Wheal et al., 1998) that the amplitude of the spike was increased in the KA-treated rats as compared with control rats, i.e. the E-S coupling was increased (Fig. 5). We also found that KA-treated rats showed, in comparison to control rats, an increase of PS2 amplitude for a given PS1 amplitude (Fig. 3D), and an increase in PS bursting (Meier and Dudek, 1996; Smith and Dudek, 2001) following the second pulse (Fig. 3 inset; Fig. 8A). The above results suggest a loss of inhibition in CA1 (Ashwood et al., 1986; Cornish and Wheal, 1989; Franck et al., 1988; Franck and Schwartzkroin, 1985), although an increase in voltage-dependent Na and Ca current activation and a decrease in K channel activation could contribute as well (Magee et al., 1998).

PSs originated at various layers in KA-treated rats

In control rats, an orthodromic PS following CA3b stimulation originated from the proximal apical dendrites (Herreras, 1990; Kloosterman et al., 2001). In KA-treated rats, most PSs following CA3b stimulation also originated from the proximal apical dendrites, but some PSs started at the CA1 basal dendrites, likely as a consequence of an increased basal dendritic excitation in KA-treated rats. In addition, the CA3b-evoked PS propagated into the distal ($>$200 μm) apical dendrites more often in KA-treated than control rats. Increase in back-propagating spikes in CA1 *in vitro* was also reported in rats after pilocarpine seizures (Bernard et al., 2001). Most distinctly, a short-latency ($<$10 ms) PS in CA1 after MPP stimulation was found exclusively in KA-treated rats and not control rats. The MPP-evoked PSs in CA1 often started from the middle and distal apical dendrites ($>$200 μm from the cell body) and propagated centripetally to the cell body layer (arrowhead in Fig. 7B). A previous study reported an enhanced population spike in CA1 in freely moving rats following perforant path stimulation within 5 days after KA injection (Fowler and Olton, 1984).

Membrane excitability at the distal dendrites was likely induced by a combination of inhibition decrease and intrinsic excitability increase. The role of EPSP is not clear, and the dendritic spikes often arose from small postsynaptic excitatory sinks (compare Fig. 7 with Fig. 6), as was observed after acute bicuculline administration (Leung and Peloquin, unpublished observation). It is known that inhibition normally suppressed the back-propagation of dendritic spike (Miles et al., 1996; Tsubokawa and Ross, 1996), while inhibition blockade may shift spike generation from the axon hillock to the apical dendrites (Golding and Spruston, 1998). A differential loss in dendritic inhibition (Cossart et al., 2001) is expected to enhance dendritic spiking in KA-treated rats, as observed in this study. A change in Ca channel density (Bernstein et al., 1999), an enhancement of Na and Ca currents in single CA1 neurons (Fass et al., 1996; Vreugdenhil and Wadman, 1994; Vreugdenhil et al., 1998), or a decrease in A-currents in the distal dendrites (Bernard et al., 2001; Magee et al., 1998) may also contribute to dendritic spiking (Magee et al., 1998).

Role of parallel and serial activation of CA1 in KA seizures

In the normal/control rat, the trisynaptic pathway from EC to CA1 provides a stronger excitation than the direct temporammonic pathway from EC to CA1 (Leung et al., 1995; Yeckel and Berger, 1998). If trisynaptic transmission in the hippocampus is the norm, the DG would act as a gate in seizure generation (Lothman, 1994), and the increase in DG inhibition after KA seizures (Buckmaster and Dudek, 1997; Milgram et al., 1991; Nusser et al., 1998; Otis et al., 1994; Tuff et al., 1983; Wu and Leung, 2001) would further fortify the gating. However, we found that there was strong, direct excitation of CA1 by the EC in the KA-treated rats (Fig. 10), and this persistent increase in EC to CA1 transmission likely contributes to an increased seizure susceptibility, bypassing the gating at the DG.

The whole entorhinal-hippocampal circuit is altered following KA treatment (Fig. 10). Basal dendritic and distal apical dendritic excitation in CA1 were more important in KA-treated rats, as compared with the dominance of the midapical dendritic excitation in control rats. In the KA-treated rat, transmission of repeated and paired signals (stimulus pulses) from the EC to the midapical dendrites of CA1 was suppressed, in part attributed to the DG (Wu and Leung, 2001). However, the overall response in CA1 following MPP stimulation was enhanced in KA-treated rats, suggesting an overall increase in throughput in the EC to CA1 circuit.

Reverberating activation via hippocampo-entorhinal loop following KA seizures

In the present study, CA3 stimulation resulted in a long latency ($\geq$20 ms) PS sink in the apical dendrites and cell layer of CA1 in KA-treated rats. The latency of the late CA1 PS was similar to that in the DG (Wu and Leung, 2001) following stimulation of CA3, suggesting that the EC projections to the DG and CA1 were activated in parallel in KA-treated rats (Fig. 10B). The increase in direct EC to CA1 excitation likely contributes to the strong hippocampo-entorhinal reverberations in KA-treated rats, but the complete multisynaptic pathway may involve CA3$\rightarrow$CA1/subiculum$\rightarrow$EC$\rightarrow$MPP$\rightarrow$CA1 (Fig. 10B). Reverberation

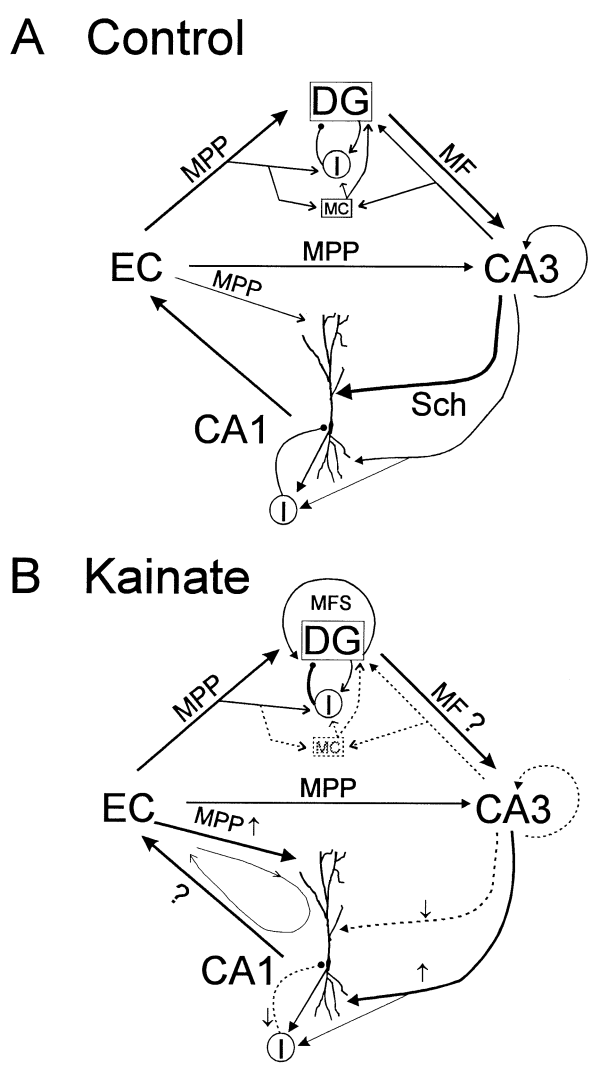

Fig. 10. Changes in the entorhinal-hippocampal circuit after kainate treatment. Excitatory synapses are indicated by an arrowhead and inhibitory connections by a solid circle. Thick arrows represent the main pathways. (A) In the control animals, the dentate gyrus (DG) receives inputs from the perforant path from the entorhinal cortex (EC); only the medial perforant path (MPP) is shown. DG projects to CA3 via mossy fibers (MF). CA3 pyramidal cells recurrently excite each other (curve with arrowhead) and project to CA1 via Schaffer collaterals (Sch). CA3 also projects back to the DG (Wu et al., 1998) and hilar interneurons. CA1 sends outputs back to the EC (and indirectly through the subiculum, not shown). EC sends direct inputs to CA3 and CA1 and collaterals to hilar interneurons and mossy cells (MC). Interneurons (I) in the DG and CA1 receive feed-forward and feedback excitation, and inhibit principal cells in the DG and CA1 through the solid black synapses. Only one type of inhibitory interneuron in DG and CA1 is shown. (B) After kainate treatment, decrease in synaptic strength is indicated by dotted lines, and increase in synaptic strength by thicker lines than in control. Question mark indicates unknown changes. CA3 pyramidal cell and mossy cell loss resulted in loss in the association input to the DG (Wu and Leung, 2001), the recurrent excitation in CA3 (in particular, CA3c) and apical dendritic excitation to CA1. However, basal dendritic excitation of CA1 and a direct EC input to the distal apical dendrites of CA1 were increased. Inhibition was decreased in CA1. Mossy fiber sprouting (MFS) is indicated by curved arrows, and inhibition was increased in the DG.

through hippocampo-entorhinal loop was proposed to sustain and amplify epileptiform activity in various preparations (Pare et al., 1992; Stringer and Lothman, 1992; Wu and Leung, 1999). As a consequence of the latter reverberant activity, synchronous epileptiform discharges may propagate from the hippocampus and the EC to the rest of the brain. EC cell loss, in particular in layer III cells that projected to CA1, was reported in human TLE and various animal models of TLE (Du et al., 1995). However, no obvious cell loss in the EC was found in the KA-treated rats of this study. Complete EC cell loss would eliminate hippocampo-entorhinal reverberations, but partial EC cell loss may increase EC excitability and contribute to the reverberations.

In conclusion, KA-treated rats showed alterations in dendritic excitatory transmission in CA1. Basal and distal apical dendritic excitation showed the largest increase after KA treatment, resulting in PSs that originated from the basal or distal apical dendrites. The increase in paired-pulse excitability in CA1 following perforant path stimulation suggests an overall proconvulsant change in the entorhinal-hippocampal circuit, characterized by robust direct entorhinal-CA1 excitation and hippocampo-entorhinal reverberations.

Acknowledgements—This work was supported by operating grants from the Medical Research Council MOP-36421 and the Natural Sciences and Engineering Research Council of Canada, and doctoral studentships to K.W. funded by Savoy Foundation and Epilepsy Canada. The multichannel silicon probes were provided by the Michigan Center for Neural Communication Technology, sponsored by NIH/NCRR grant P41 RR09754-04.

REFERENCES

Adams B, Sazgar M, Osehobo P, Van der Zee CE, Diamond J, Fahnestock M, Racine RJ (1997) Nerve growth factor accelerates seizure development, enhances mossy fiber sprouting, and attenuates seizure-induced decreases in neuronal density in the kindling model of epilepsy. J Neurosci 17:5288–5296.

Andersen P, Bliss TV, Skrede KK (1971) Lamellar organization of hippocampal pathways. Exp Brain Res 13:222–238.

Ashwood TJ, Lancaster B, Wheal HV (1986) Intracellular electrophysiology of CA1 pyramidal neurones in slices of the kainic acid lesioned hippocampus of the rat. Exp Brain Res 62:189–198.

Ashwood TJ, Wheal HV (1986) Extracellular studies on the role of N-methyl-D-aspartate receptors in epileptiform activity recorded from the kainic acid-lesioned hippocampus. Neurosci Lett 67:147–152.

Ashwood TJ, Wheal HV (1986) Loss of inhibition in the CA1 region of the kainic acid lesioned hippocampus is not associated with changes in postsynaptic responses to GABA. Brain Res 367:390–394.

Bekenstein JW, Lothman EW (1993) Dormancy of inhibitory interneurons in a model of temporal lobe epilepsy. Science 259:97–100.

Bernard C, Wheal HV (1995) Plasticity of AMPA and NMDA receptor-mediated epileptiform activity in a chronic model of temporal lobe epilepsy. Epilepsy Res 21:95–107.

Bernard C, Poolos NP, Johnston D (2001) A-type K channel control of dendritic excitability in experimental epilepsy. Neurosci Abstr 27 #559.1.

Bernstein GM, Mendonca A, Wadia J, Burnham WM, Jones OT (1999) Kindling induces an asymmetric enhancement of N-type Ca channel density in the dendritic fields of the rat hippocampus. Neurosci Lett 268:155–158.

Best N, Mitchell J, Baimbridge KG, Wheal HV (1993) Changes in parvalbumin-immunoreactive neurons in the rat hippocampus following a kainic acid lesion. Neurosci Lett 155:1–6.

Best N, Mitchell J, Wheal HV (1994) Ultrastructure of parvalbumin-immunoreactive neurons in the CA1 area of the rat hippocampus following a kainic acid injection. Acta Neuropathol (Berl) 87:187–195.

Brooks-Kayal AR, Shumate MD, Jin H, Rikhter TY, Coulter DA (1998) Selective changes in single cell GABA(A) receptor subunit expression and function in temporal lobe epilepsy. Nat Med 4:1166–1172.

Buckmaster PS, Dudek FE (1997) Network properties of the dentate gyrus in epileptic rats with hilar neuron loss and granule cell axon reorganization. J Neurophysiol 77:2685–2696.

Buckmaster PS, Schwartzkroin PA (1995) Interneurons and inhibition in the dentate gyrus of the rat in vivo. J Neurosci 15:774–789.

Canning KJ, Wu K, Peloquin P, Kloosterman F, Leung LS (2000) Physiology of the entorhinal and perirhinal projections to the hippocampus studied by current source density analysis. Ann N Y Acad Sci 911:55–72.

Cornish SM, Wheal HV (1989) Long-term loss of paired pulse inhibition in the kainic acid-lesioned hippocampus of the rat. Neuroscience 28:563–571.

Cossart R, Dinocourt C, Hirsch JC, Merchan-Perez A, De Felipe J, Ben Ari Y, Esclapez M, Bernard C (2001) Dendritic but not somatic GABAergic inhibition is decreased in experimental epilepsy. Nat Neurosci 4:52–62.

Du F, Eid T, Lothman EW, Kohler C, Schwarcz R (1995) Preferential neuronal loss in layer III of the medial entorhinal cortex in rat models of temporal lobe epilepsy. J Neurosci 15:6301–6313.

Esclapez M, Hirsch JC, Ben Ari Y, Bernard C (1999) Newly formed excitatory pathways provide a substrate for hyperexcitability in experimental temporal lobe epilepsy. J Comp Neurol 408:449–460.

Fass GC, Vreugdenhil M, Wadman WJ (1996) Calcium currents in pyramidal CA1 neurons in vitro after kindling epileptogenesis in the hippocampus of the rat. Neuroscience 75:57–67.

Fowler KR, Olton DS (1984) Recovery of function following injections of kainic acid: behavioral, electrophysiological and neuroanatomical correlates. Brain Res 321:21–32.

Franck JE, Kunkel DD, Baskin DG, Schwartzkroin PA (1988) Inhibition in kainate-lesioned hyperexcitable hippocampi: physiologic, autoradiographic, and immunocytochemical observations. J Neurosci 8:1991–2002.

Franck JE, Schwartzkroin PA (1985) Do kainate-lesioned hippocampi become epileptogenic? Brain Res 329:309–313.

Freeman JA, Nicholson C (1975) Experimental optimization of current source-density technique for anuran cerebellum. J Neurophysiol 38:369–382.

Freund TF, Buzsaki G (1996) Interneurons of the hippocampus. Hippocampus 6:347–470.

Gibbs JW III, Shumate MD, Coulter DA (1997) Differential epilepsy-associated alterations in postsynaptic GABA(A) receptor function in dentate granule and CA1 neurons. J Neurophysiol 77:1924–1938.

Golarai G, Sutula TP (1996) Functional alterations in the dentate gyrus after induction of long-term potentiation, kindling, and mossy fiber sprouting. J Neurophysiol 75:343–353.

Golding NL, Spruston N (1998) Dendritic sodium spikes are variable triggers of axonal action potentials in hippocampal CA1 pyramidal neurons. Neuron 21:1189–1200.

Herreras O (1990) Propagating dendritic action potential mediates synaptic transmission in CA1 pyramidal cells in situ. J Neurophysiol 64:1429–1441.

Hirsch JC, Agassandian C, Merchan-Perez A, Ben Ari Y, De Felipe J, Esclapez M, Bernard C (1999) Deficit of quantal release of GABA in experimental models of temporal lobe epilepsy. Nat Neurosci 2:499–500.

Ishizuka N, Weber J, Amaral DG (1990) Organization of intrahippocampal projections originating from CA3 pyramidal cells in the rat. J Comp Neurol 295:580–623.

Kaibara T, Leung LS (1993) Basal versus apical dendritic long-term potentiation of commissural afferents to hippocampal CA1: a current-source density study. J Neurosci 13:2391–2404.

Kloosterman F, Peloquin P, Leung LS (2001) Apical and basal orthodromic population spikes in hippocampal CA1 in vivo show different origins and patterns of propagation. J Neurophysiol 86:2435–2444.

Leung LS (1990) Field potentials in the central nervous system: recording, analysis and modeling. In: Neurophysiological techniques, Vol. 15. (Boulton AA, Baker GB, Vanderwolf CH, eds), pp 313–369. Clifton, NJ: Humana.

Leung LS, Roth L, Canning KJ (1995) Entorhinal inputs to hippocampal CA1 and dentate gyrus in the rat: a current-source-density study. J Neurophysiol 73:2392–2403.

Leung LS, Shen B, Sutherland R, Wu C, Wu K, Zhao D (1998) Long-lasting behavioral and electrophysiological effects induced by partial hippocampal kindling. In: Kindling 5 (Corcoran ME, Moshe SL, eds), pp 395–408. New York: Plenum Press.

Li XG, Somogyi P, Ylinen A, Buzsaki G (1994) The hippocampal CA3 network: an in vivo intracellular labeling study. J Comp Neurol 339:181–208.

Longo BM, Mello LE (1998) Supragranular mossy fiber sprouting is not necessary for spontaneous seizures in the intrahippocampal kainate model of epilepsy in the rat. Epilepsy Res 32:172–182.

Lothman EW (1994) Seizure circuits in the hippocampus and associated structures. Hippocampus 4:286–290.

Magee J, Hoffman D, Colbert C, Johnston D (1998) Electrical and calcium signaling in dendrites of hippocampal pyramidal neurons. Annu Rev Physiol 60:327–346.

McKinney RA, Debanne D, Gahwiler BH, Thompson SM (1997) Lesion-induced axonal sprouting and hyperexcitability in the hippocampus in vitro: implications for the genesis of posttraumatic epilepsy. Nat Med 3:990–996.

Meier CL, Dudek FE (1996) Spontaneous and stimulation-induced synchronized burst afterdischarges in the isolated CA1 of kainate-treated rats. J Neurophysiol 76:2231–2239.

Miles R, Toth K, Gulyas AI, Hajos N, Freund TF (1996) Differences between somatic and dendritic inhibition in the hippocampus. Neuron 16:815–823.

Milgram NW, Yearwood T, Khurgel M, Ivy GO, Racine R (1991) Changes in inhibitory processes in the hippocampus following recurrent seizures induced by systemic administration of kainic acid. Brain Res 551:236–246.

Morin F, Beaulieu C, Lacaille JC (1998) Cell-specific alterations in synaptic properties of hippocampal CA1 interneurons after kainate treatment. J Neurophysiol 80:2836–2847.

Morin F, Beaulieu C, Lacaille JC (1999) Alterations of perisomatic GABA synapses on hippocampal CA1 inhibitory interneurons and pyramidal cells in the kainate model of epilepsy. Neuroscience 93:457–467.

Nadler JV, Perry BW, Gentry C, Cotman CW (1980) Loss and reacquisition of hippocampal synapses after selective destruction of CA3-CA4 afferents with kainic acid. Brain Res 191:387–403.

Nusser Z, Hajos N, Somogyi P, Mody I (1998) Increased number of synaptic GABA(A) receptors underlies potentiation at hippocampal inhibitory synapses. Nature 395:172–177.

Okazaki MM, Molnar P, Nadler JV (1999) Recurrent mossy fiber pathway in rat dentate gyrus: synaptic currents evoked in presence and absence of seizure-induced growth. J Neurophysiol 81:1645–1660.

Otis TS, De Koninck Y, Mody I (1994) Lasting potentiation of inhibition is associated with an increased number of gamma-aminobutyric acid type A receptors activated during miniature inhibitory postsynaptic currents. Proc Natl Acad Sci USA 91:7698–7702.

Pare D, deCurtis M, Llinas R (1992) Role of the hippocampal-entorhinal loop in temporal lobe epilepsy: extra- and intracellular study in the isolated guinea pig brain in vitro. J Neurosci 12:1867–1881.

Perez Y, Morin F, Beaulieu C, Lacaille JC (1996) Axonal sprouting of

CA1 pyramidal cells in hyperexcitable hippocampal slices of kainate-treated rats. Eur J Neurosci 8:736–748.
Roth LR, Leung LS (1995) Difference in LTP at basal and apical dendrites of CA1 pyramidal neurons in urethane-anesthetized rats. Brain Res 694:40–48.
Simpson LH, Wheal HV, Williamson R (1991) The contribution of non-NMDA and NMDA receptors to graded bursting activity in the CA1 region of the hippocampus in a chronic model of epilepsy. Can J Physiol Pharmacol 69:1091–1098.
Smith BN, Dudek FE (2001) Short- and long-term changes in CA1 network excitability after kainate treatment in rats. J Neurophysiol 85:1–9.
Stringer JL, Lothman EW (1992) Reverberatory seizure discharges in hippocampal-parahippocampal circuits. Exp Neurol 116:198–203.
Tsubokawa H, Ross WN (1996) IPSPs modulate spike backpropagation and associated [Ca2+]i changes in the dendrites of hippocampal CA1 pyramidal neurons. J Neurophysiol 76:2896–2906.
Tsunashima K, Schwarzer C, Kirchmair E, Sieghart W, Sperk G (1997) GABA(A) receptor subunits in the rat hippocampus III: altered messenger RNA expression in kainic acid-induced epilepsy. Neuroscience 80:1019–1032.
Tuff LP, Racine RJ, Adamec R (1983) The effects of kindling on GABA-mediated inhibition in the dentate gyrus of the rat. I. Paired-pulse depression. Brain Res 277:79–90.
Turner DA, Wheal HV (1991) Excitatory synaptic potentials in kainic acid-denervated rat CA1 pyramidal neurons. J Neurosci 11:2786–2794.
Vreugdenhil M, Wadman WJ (1994) Kindling-induced long-lasting enhancement of calcium current in hippocampal CA1 area of the rat: relation to calcium-dependent inactivation. Neuroscience 59:105–114.
Vreugdenhil M, Faas GC, Wadman WJ (1998) Sodium currents in isolated rat CA1 neurons after kindling epileptogenesis. Neuroscience 86:99–107.
Wheal HV, Bernard C, Chad JE, Cannon RC (1998) Pro-epileptic changes in synaptic function can be accompanied by pro-epileptic changes in neuronal excitability. Trends Neurosci 21:167–174.
Williams S, Vachon P, Lacaille JC (1993) Monosynaptic GABA-mediated inhibitory postsynaptic potentials in CA1 pyramidal cells of hyperexcitable hippocampal slices from kainic acid-treated rats. Neuroscience 52:541–554.
Wilson CL, Khan SU, Engel J Jr, Isokawa M, Babb TL, Behnke EJ (1998) Paired pulse suppression and facilitation in human epileptogenic hippocampal formation. Epilepsy Res 31:211–230.
Witter MP, Wouterlood FG, Naber PA, van Haeften T (2000) Anatomical organization of the parahippocampal-hippocampal network. Ann N Y Acad Sci 911:1–24.
Wong RKS, Traub RD (1983) Synchronized burst discharge in disinhibited hippocampal slice. I. Initiation in CA2-CA3 region. J Neurophysiol 49:442–458.
Wu K, Leung LS (1996) Enhancement of hippocampal excitation by CA3 stimulation in kainate-seized rats: a current source density study. Neurosci Abstr 22:2103.
Wu K, Leung LS (1999) Enhancement of multisynaptic transmission through the hippocampo-entorhino-hippocampal loop in partially kindled rats in vivo. Neurosci Abstr 25:1351.
Wu K, Canning KJ, Leung LS (1998) Functional interconnections between CA3 and the dentate gyrus revealed by current source density analysis. Hippocampus 8:217–230.
Wu K, Leung LS (2001) Enhanced but fragile inhibition in the dentate gyrus in vivo in the kainic acid model of temporal lobe epilepsy: a study using current source density analysis. Neuroscience 104: 379–396.
Wu LG, Saggau P (1997) Presynaptic inhibition of elicited neurotransmitter release. Trends Neurosci 20:204–212.
Wuarin JP, Dudek FE (2001) Excitatory synaptic input to granule cells increases with time after kainate treatment. J Neurophysiol 85: 1067–1077.
Yeckel MF, Berger TW (1998) Spatial distribution of potentiated synapses in hippocampus: dependence on cellular mechanisms and network properties. J Neurosci 18:438–450.
Zhao D, Leung LS (1991) Effects of hippocampal kindling on paired-pulse response in CA1 in vitro. Brain Res 564:220–229.
Zucker RS (1989) Short-term synaptic plasticity. Annu Rev Neurosci 12:13–31.

(Accepted 27 June 2002)